IDO-14553

MASTER

CHEMICAL PROCESSING TECHNOLOGY QUARTERLY PROGRESS REPORT October – December, 1960

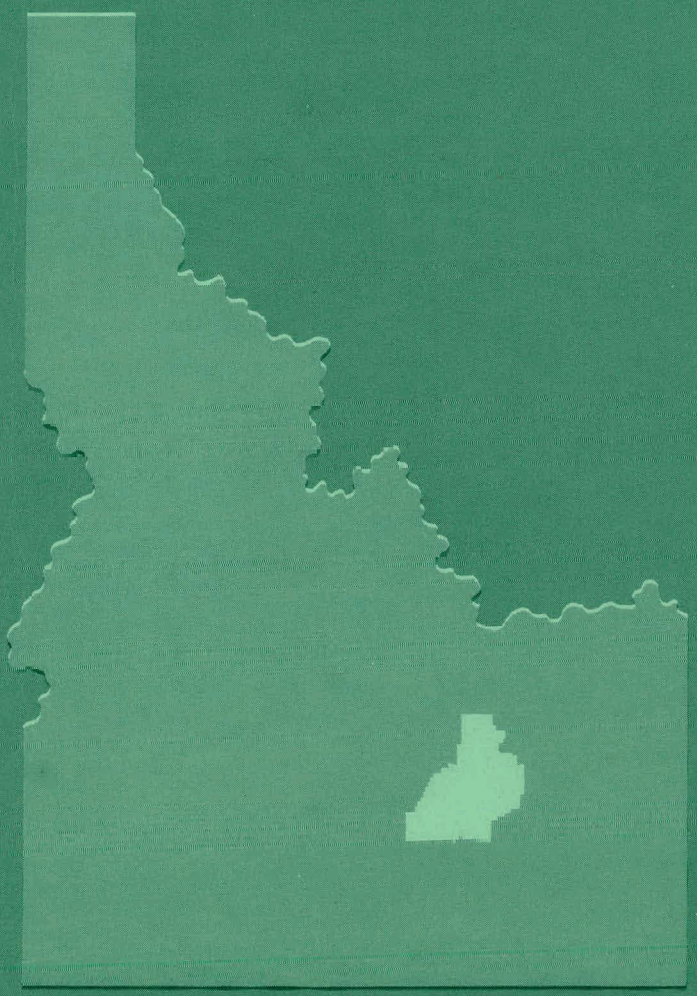

PHILLIPS PETROLEUM COMPANY

ATOMIC ENERGY DIVISION

NATIONAL REACTOR TESTING STATION

US ATOMIC ENERGY COMMISSION

DISCLAIMER

PRICE $1.75

Available from the
Office of Technical Services
U. S. Department of Commerce
Washington 25, D. C.

Printed in USA

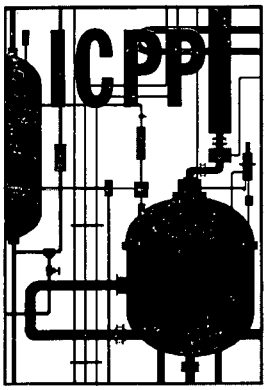

IDAHO CHEMICAL PROCESSING PLANT

IDO-14553
AEC Research and Development Report
General, Miscellaneous, and Progress Reports
TID-4500 (16th Ed.)
Issued: May 15, 1961

CHEMICAL PROCESSING TECHNOLOGY

QUARTERLY PROGRESS REPORT

OCTOBER - DECEMBER 1960

J. R. Huffman
Assistant Manager, Technical

J. A. McBride
Technical Director

C. M. Slansky
Chemical Development

F. M. Warzel
Process Development

J. R. Bower
Editor

PHILLIPS
PETROLEUM
COMPANY

Atomic Energy Division

Contract AT(10-1)-205
Idaho Operations Office
U. S. ATOMIC ENERGY COMMISSION

PAGES 2 to 3

WERE INTENTIONALLY

LEFT BLANK

Previous Reports in Series:

IDO-14324
IDO-14337
IDO-14350
IDO-14354
IDO-14362
IDO-14364
IDO-14383
IDO-14385
IDO-14391
IDO-14400
IDO-14410
IDO-14419
IDO-14422
IDO-14430
IDO-14443
IDO-14453
IDO-14457
IDO-14467
IDO-14471
IDO-14494
IDO-14509
IDO-14512
IDO-14514
IDO-14520
IDO-14526
IDO-14530
IDO-14534
IDO-14540

CHEMICAL PROCESSING TECHNOLOGY

QUARTERLY PROGRESS REPORT

October-December 1960

by

J. R. Bower, Editor

TABLE OF CONTENTS

		Page
I.	SUMMARY	11
II.	ICPP OPERATIONAL SCHEDULE, PERFORMANCE AND PROBLEMS	15
	A. ICPP Processing Schedule	15
	B. Plutonium Contamination of Solvent	16
III.	AQUEOUS PROCESSING STUDIES	19
	A. Aqueous Zirconium Fuel Processing	19
	1. Barium Fluozirconate Precipitation Process	19
	2. Additional Zirconium Precipitation Processes	21
	a. Zirconium Removal with Salicylic Acid	21
	b. Zirconium Removal with Paraformaldehyde and/or Formic Acid	22
	c. Zirconium Removal with Sodium Formate	23
	B. Aqueous Ceramic Fuel Processing	25
	1. Chemical Reprocessing of $BeO-UO_2$	25
IV.	WASTE CALCINATION DEVELOPMENT AND DEMONSTRATION	28
	A. Research and Development in the Pilot Plant	29
	1. Performance of Feed Nozzles in the Two-Foot-Square Calciner	29
	2. Absolute Density and Nitrate Content of Alumina Produced in the Two-Foot-Square Calciner	32
	3. Intra-Particle Porosity of Calcine	33
	4. Alpha Alumina Behavior in Calcine	33
	B. Laboratory Investigations	35
	1. Calcination of Aluminum Nitrate Wastes	35
	2. Calcination of Zirconium-Fluoride Wastes	43

TABLE OF CONTENTS (Continued)

		Page
	C. Demonstrational Waste Calcining Facility	44
	1. Program Planning and Data Correlation	44
	2. Technical Surveillance	44
V.	NEW WASTE TREATMENT METHODS	47
	A. Removal of Long-Lived Radioisotopes from Waste Solutions	47
	B. Mercury Cathode Electrolysis of Stainless Steel Wastes	49
VI.	ELECTROLYTIC DISSOLUTION SYSTEMS	53
	A. Electrolytic Dissolution of Stainless Steel in Nitric Acid	53
	1. Potential-Current Density Relationships in the Stainless Steel-Nitric Acid System	53
	2. Electrolytic Reduction of Nitric Acid	55
	3. Effect of Cell and Electrode Geometry on Current Density Distribution-Analog Simulation of Current Paths	55
	4. Embrittlement of Niobium Used as a Cathode	58
	5. Corrosion Behavior of Electrolytic Dissolver Product Solution	59
	B. Electrolytic Disintegration of Zirconium-Base Alloys	60
	C. Single Electrode Potential Measurements as an Indication of Cathode Corrosion	61
VII.	THE ARCO PROCESS - DISSOLUTION OF FUEL ALLOYS IN MOLTEN CHLORIDES	63
	A. Dissolution of UO_2 in the $PbCl_2$-Cl_2 System	63
	B. Dissolution of UO_2 in the $PbCl_2$-Cl_2 System Catalyzed by Copper	64
	C. Dissolution of Niobium in Molten Lead Chloride	66
VIII.	EQUIPMENT DEVELOPMENT	68
	A. Direct Air Pulsing of Extraction Columns	68
	B. Large Vessel Criticality Control	71
IX.	REPORTS AND PUBLICATIONS ISSUED DURING THE QUARTER	74
X.	REFERENCES	75

LIST OF TABLES

Table	Title	Page
1	Barium-140 Production at ICPP, October-December, 1960. .	15
2	Temperature Profile in Packed Bed.	17
3	Fission Product Behavior During Precipitation of Barium Fluozirconate from STR Dissolver Solutions.	21
4	Zirconium Recovery from Simulated STR Dissolver Solution	22
5	Recovery of Uranium from Pulverized Ceramic Fuel by Leaching with Nitric Acid.	26
6	Recovery of Uranium from Pulverized Ceramic Fuel - Effect of Particle Size	26
7	Recovery of Uranium from Pulverized Ceramic Fuel by Successive Leachings	27
8	Calcining Conditions for the Performance Studies of the Redesigned DWCF Feed Nozzles	31
9	Similar Operating Conditions in Runs Which Exhibited Early Peak in Product Alpha Alumina Content	35
10	Results of Exposing Amorphous Alumina to Nitric Acid, Air, and Water Vapor at Elevated Temperatures	37
11	Crystal Composition of Residues Resulting from the Acid Digestion of Amorphous (to X-Ray) Calcined Alumina. .	39
12	Results of Calcination of Synthetic Process Wastes Containing Zirconium Fluoride	44
13	Feed Nozzle Tip Erosion Results.	46
14	Adsorption of Cesium by APM from Synthetic ICPP Waste at 25° C	48
15	Adsorption of Strontium from Acidic Solutions by Ion Exchange Resins at 25° C	49
16	Corrosion in Electrolytic Dissolver Product Solution . .	59
17	Effect of Temperature on Rate of Electrolytic Disintegration of Zircaloy-2.	61
18	Correlation of Single Electrode Potential and Cathodic Corrosion During Electrolytic Disintegration of Zircaloy.	61

LIST OF FIGURES

Figure	Title	Page
1	Effect of Packing Height and Solvent-Steam Ratio on Solvent Residue Rate.	17
2	Effect of TBP Concentration and Solvent-Steam Ratio on Solvent Residue Rate.	17
3	Solvent-Steam Ratio and Temperature Requirements for Elimination of Column Bottoms (Residue) Flow . .	18
4	Effect of Sodium Formate Concentration on Zirconium Recovery.	23
5	Effect of Reaction Time on Zirconium Recovery	23
6	Comparison of Various Nozzle Caps Used on Spraying Systems Company Type 1/2 J Nozzle in the Two-Foot-Square Calciner.	30
7	Variation in Nitrate Content of Alumina Product	32
8	Variation in Absolute Density of Alumina Product. . . .	32
9	Variation in Alpha Alumina Content of Alumina Product .	34
10	Conversion of Amorphous Alumina to Alpha Alumina at 400-600° C	38
11	Conversion of Amorphous Alumina to Alpha Alumina at 400-500° C (Logarithmic Plot). .	39
12	Electron Diffraction Pattern of Amorphous (to X-Ray) Alumina.	41
13	Same as Figure 12 After Four-Minute Exposure to 40 Kv Electrons	41
14	Amorphous Alumina - Magnification 100,000	42
15	Same as Figure 14 - Magnification 20,000.	42
16	90% Alpha Alumina - Magnification 38,000.	42
17	Same as Figure 16 - Magnification 10,000.	42
18	Equilibrium Distribution for Cesium in Synthetic ICPP Waste.	49

LIST OF FIGURES (Continued)

Figure	Title	Page
19	Removal of Stainless Steel Metal Ions from Synthetic Waste Solution at 25° C as a Function of Initial Sulfuric Acid Concentration.	51
20	Removal of Stainless Steel Metal Ions from Synthetic Waste Solution at 35° C as a Function of Ampere-Hours	51
21	Potential-Current Density Relationships at 25° C for Type 304 Stainless Steel in the Transpassive Region as a Function of Nitric Acid Concentration. .	54
22	Current Limitation Between Isopots.	57
23	Isopotential Lines in Sector of Uniform Geometry. . . .	57
24	Isopotential Lines in Non-Uniform Geometry.	57
25	Isopotential Lines in Non-Uniform Geometry.	57
26	Dissolution Rate of UO_2 in Molten Lead Chloride at 550° C as a Function of Cl_2 Flow Rate	65
27	Dissolution Rate of UO_2 in Molten Lead Chloride at 550° C as a Function of Copper Concentration. . .	65
28	Weight Loss of Niobium in Lead Chloride as a Function of Temperature	67
29	Schematic of Air Pulser Test System	69
30	Air Pulser Air Supply System.	70
31	Extraction Column Air Pulser Settings	72

THIS PAGE

WAS INTENTIONALLY

LEFT BLANK

CHEMICAL PROCESSING TECHNOLOGY

QUARTERLY PROGRESS REPORT

October-December 1960

J. R. Bower, Editor

I. SUMMARY

While the Idaho Chemical Processing Plant was not operating on fuel recovery during this period, significant changes were made in processing equipment in preparation for forthcoming operations. Remote head diaphragm pumps feeding the head end evaporator and the first cycle extraction columns were removed and replaced with air lifts, reflecting the successful operation of air lifts previously installed in several locations in an effort to reduce the continual operating difficulties associated with remote pumps. A direct air pulsing system was installed on the first cycle extraction column, in anticipation of eliminating the ever-troublesome, remote head pulsing system, which, for the present, was left installed in stand-by condition. Necessary in-cell work was also completed to permit rapid future installation of the air pulsing system on the scrub and strip columns if the first application proves as successful as anticipated on the basis of pilot plant operation.

Barium-140 production was continued on schedule, without incident, averaging approximately 60 per cent recovery of high quality product. Operations at the Demonstrational Waste Calcining Facility were limited by the existence of equipment and design deficiencies brought out in the course of extensive tests on individual system components. Progress is reported on the use of a packed steam stripper to free waste solvent from low concentrations of plutonium prior to incineration.

In continuing studies of aqueous zirconium processing, directed at reduction of solution volumes to be processed and stored as waste through separation of bulk zirconium from dissolver solutions, confirmation was made of a previous observation that the use of a mixed precipitant (barium fluoride-barium nitrate) achieved better separation of fission products and more complete precipitation of zirconium than was obtained by the use of barium nitrate alone; fission product zirconium and yttrium, as well as the previously-reported strontium and cerium, were largely carried with the bulk zirconium precipitate, while niobium, cesium, and ruthenium remained largely in solution. An alternate method for removing zirconium from hydrofluoric acid process solutions -- addition of sodium formate, in a 2/1 mole ratio with the zirconium, to a properly-adjusted solution (uranium in the +6 oxidation state) -- led to a rapid (five minutes) and nearly-quantitative precipitation of

zirconium and fluoride, with a uranium loss of only 0.1 per cent. Alternatives proving to be less desirable included refluxing with paraformaldehyde and/or formic acid, which gave an 80 per cent recovery of zirconium after 6 hours, and precipitation with salicylic acid, which gave less than 25 per cent recovery.

Recovery of uranium from a beryllia-uranium dioxide ceramic fuel by a grinding-leaching technique, using boiling nitric acid (3M to 15.7M) as the leaching agent, reached 75-80 per cent, requiring 2 or more hours' contact time with material preferably in the 50-200 mesh size range.

Pilot plant studies of the fluidized bed calcination process for reduction of radioactive liquid wastes to the more-easily-stored solid form have continued with investigation, in the two-foot-square calciner, of feed spray nozzles designed for use in the Demonstrational Waste Calcining Facility. The most suitable nozzle cap design has yet to be determined; flat-faced nozzles have shown excessive erosion rates; an extended convergent cone tip has shown excellent erosion resistance, but a relatively narrow operating range with respect to air-liquid ratios; an extended divergent cone tip proved inoperable in continuous runs, at any air-liquid ratio attainable in the test equipment, due to uncontrollable particle growth which interfered with heat transfer. Recent runs have indicated that the nitrate content and absolute density of the alumina produced in the pilot plant calciner are related to calcining temperature and/or feed composition as well as to alpha alumina content, as reported previously; comparison of products with similar alpha alumina content show that calcination of a 1.95M aluminum nitrate solution at 500° C yields alumina with a lower nitrate content, lower density, and higher porosity than calcination of a 1.29M solution at 400° C.

A newly-observed phenomenon in regard to the physical structure of the alumina produced during operation of the fluidized bed calciner during the past few runs has been a rapid increase in the alpha alumina content of the bed (from 12 per cent in the starting bed to a high of 36 to 48 per cent) during the first 6 to 18 hours of operation, followed by a gradual decline to a value between 4 and 12 per cent after 100 hours of operation. In contrast to this, in earlier runs, beds having an alpha alumina content slightly above 28 per cent were unstable and were transformed rapidly to beds containing over 60 per cent alpha alumina, with no evidence of any retrogression to a lower level. Temperature (400° C vs 500° C) appears to be a factor involved, but complete evaluation of the pilot plant variables involved has not yet been accomplished. Laboratory exploration of the variables of the system has demonstrated that a combination of the presence of sodium nitrate and an atmosphere containing air, water vapor, and oxides of nitrogen markedly increases the rate of formation of alpha alumina from amorphous alumina in the 400-600° C range, but the kinetics and mechanism of the reaction remain to be determined. Exposure of samples of alumina from the pilot plant calciner to the electron beam in an electron microscope caused apparent changes in crystal structure (as indicated by sharpening of rings in diffraction patterns) within a few minutes. More recent investigation has indicated that this effect, if real, is not caused by radiation.

Calcination of fluoride-containing waste solutions typical of those obtained from hydrofluoric acid dissolution of zirconium fuel has been accomplished at temperatures of 400-535° C, without volatilization of detectable quantities (0.25 per cent) of fluoride, after overnight treatment with calcium oxide chemically equivalent to the fluoride content. This gives promise to utilization of the stainless steel Demonstrational Waste Calcining Facility for treatment of zirconium fuel processing wastes.

Additional studies on removal of long-lived radioisotopes from waste solutions (a program directed at simplifying long-term storage and disposal problems) demonstrated that the distribution coefficient for cesium adsorption from synthetic ICPP waste by ammonium phosphomolybdate remained high (approximately 3600) over a range of cesium concentrations from tracer level to that existing in ICPP waste (approximately 0.06 mg/ml). Preliminary experiments on the adsorption of strontium from acidic solutions (0.1N HNO_3, HCl, H_2SO_4, HF) by Amberlite resins gave adsorption coefficients in excess of 1000 in the absence of interfering salt ions; in a 0.1N nitric acid solution containing 1M aluminum nitrate, the coefficient for Amberlite 200 (the only resin tested under such conditions) fell to 66.

Continued investigation of removal, by mercury cathode electrolysis, of iron, nickel, and chromium from waste solutions resulting from processing of stainless steel reactor fuels (in an effort to achieve economies over the current high-volume, liquid-waste storage practice) has indicated that the most effective separation, at room temperature, was achieved in sulfuric acid concentrations of less than 0.5M or greater that 2.0M; an apparent inhibiting effect of 1M sulfuric acid on the removal of the alloy metal ions was eliminated by operating at 35° C. Preliminary experiments indicated that mercury cathode amalgams containing approximately 2 per cent stainless steel could be prepared before reaching a semi-solid state which would require treatment to remove the base metals.

With electrolytic dissolution in nitric acid having been demonstrated as applicable to a wide variety of stainless steel and other alloy materials, study has been directed at fundamental reactions occurring in the dissolver and effect of cell and electrode geometry, factors which are important to both cell design and operation. A study of the electrolytic dissolution of Type 304 stainless steel as a function of electrode potential and nitric acid concentration (1-14M) revealed a varied pattern of limiting current density relationships influenced by concentration polarization or film formation. Preliminary experiments on the reduction of nitric acid at a gold cathode are underway in an attempt to isolate and study the individual reactions involved in the complex sequence. An analog simulation technique was used to study current distribution in a proposed electrolytic dissolver involving non-symmetrical arrangements not readily adaptable to mathematical analysis. Current distribution on the dissolver cathode, through the dissolver basket, on non-symmetrical anodes, and the actual path followed by the current in the dissolver were studied by tracing lines of equipotential on an analog, representing a cross section of the dissolver,

constructed of conductive rubber sheeting with appropriate electrodes and basket interferences incorporated.

Preliminary results of continuing tests on the corrosion resistance of materials of construction toward electrolytic dissolver solutions indicate excellent resistance for titanium (0.002 mils/month), moderate corrosion rates for stainless steels (3.5 to 5 mils/month), and a prohibitive corrosion rate for Inconel (61 mils/month) in a boiling 1M nitric acid solution containing 75 g/l of dissolved Type 304 stainless steel. A niobium cathode in an electrolytic dissolver (dissolving stainless steel in boiling 8M nitric acid) did not absorb hydrogen under these conditions in a 1000-hour test, indicating that it should not undergo hydrogen embrittlement in such service.

Electrolytic disintegration of Zircaloy-2 in 8M nitric acid at 60° C has been demonstrated to proceed at a penetration rate of 0.6 mm/hr and a current efficiency of approximately 100 per cent with separation of the major portion of the zirconium as ZrO_2, although a smaller portion remains in solution. Preliminary work on the electrolytic disintegration of Zircaloy-2 in neutral systems (8M sodium nitrate, 8M ammonium nitrate, 2.3M aluminum nitrate) indicates that the zirconium can be precipitated nearly quantitatively as ZrO_2. Advantages of operating in the neutral system would include (a) uranium zirconium separation, (b) reduction of cathodic corrosion, and (c) elimination of nitric acid-zirconium explosion hazard. The possibility of obtaining prompt indication of cathode corrosion in an operating electrolytic dissolver is being explored by correlation of cathode potential measurements made with a Luggin probe.

Successful adaptation of the ARCO Process to dissolution of UO_2 was achieved by addition of copper (as either CuCl or copper metal) to the $PbCl_2$-Cl_2 system to act as a carrier during the chlorination. A dissolution rate of 69 mg/(cm^2)(min) was attained in a molten bath (550° C) of $PbCl_2$ (containing 10 mole per cent copper) at a chlorine feed rate of 64 mg/min; this rate is approximately 100-fold higher than that obtained in the absence of copper. Preliminary experiments indicate low dissolution rates (<0.5 mg/$(cm)^2$(min)) for niobium (a fission product contaminant) in molten lead chloride.

As the initial step in an experimental study of large vessel criticality control directed at safe containment of enriched uranium solutions in large diameter vessels (in order to minimize the hazard of accidentally accumulating unsafe quantitites or concentrations of uranium in enlarged portions of equipment, which are difficult to eliminate in a large-capacity enriched-uranium processing plant), a prefabricated cartridge of adjustable boron stainless steel plates has been designed for use in a 36" diameter x 48" high tank, and a series of neutron multiplication tests is planned to verify calculations entering into the design.

II. ICPP OPERATIONAL SCHEDULE, PERFORMANCE, AND PROBLEMS

A. ICPP Processing Schedule, J. R. Bower

The Idaho Chemical Processing Plant did not operate on fuel recovery during this period. Extraction feed preparation equipment was modified to assure more reliable operation in the future. Remote head diaphragm pumps feeding the head end evaporator and the first cycle extraction columns were removed and replaced with air lifts, reflecting the successful operation of air lifts previously installed in several locations in an effort to reduce the continual operating difficulties associated with remote pumps. Few remote head diaphragm pumps remain in service at the ICPP in the processing system for aluminum elements. The heat exchanger bundle in the head end evaporator was removed and replaced with a larger capacity, titanium tube bundle, since corrosion evaluation had indicated that the original Type 347 stainless steel exchanger was approaching its predicted life expectancy. Standpipe legs were added to the first cycle extraction, scrub and strip columns to enable use of direct air pulsing in place of remote head diaphragm pulsers (see Section VIII, this report). A complete installation of control and air pulsing equipment was made on the extraction column to test the principle under plant operating conditions. All in-cell work was completed on the other two columns, leaving only out-of-cell work to be completed at some time in the future, if complete conversion to direct air pulsing is proved to be desirable. In addition to these major modifications, desirable changes were made in valve, jet, and line locations to simplify future plant decontamination. A number of oversized trombone-type coolers were also replaced with simple, straightline, double-pipe coolers.

Reconcentration of the contents of a 300,000-gallon waste storage tank containing second and third cycle extraction wastes and miscellaneous process equipment wastes was completed. A total of 293,626 gallons of waste solution was concentrated to 151,286 gallons and returned to storage, thus recovering use of approximately one-half tank for future waste disposal.

Operations at the Demonstrational Waste Calcining Facility were limited by the existence of equipment and design deficiencies brought out in the course of extensive tests on individual system components. Pending design modifications and delays in delivery of necessary equipment make the startup schedule indefinite.

Two barium-140 product runs were completed without incident, with the customer reporting product quality to be excellent. Product recovery was as listed in Table 1.

TABLE 1

BARIUM-140 PRODUCTION AT ICPP, OCTOBER-DECEMBER, 1960

Run No.	Curies	Per Cent Recovery
048	31,800	60.0
049	25,400	60.6

B. Plutonium Contamination of Solvent, H. V. Chamberlain, Problem Leader
C. R. Ford

The Cold Pilot Plant program to study the feasibility of continuous steam stripping of TBP-Amsco 125-90W solutions from non-volatile material (in order to free waste solvent of plutonium prior to incineration) has been completed. Previously-reported pilot plant data[1] were obtained in a 4-inch diameter column with an 8-foot packed section, using 30 per cent TBP-Amsco at solvent rates of 6.5, 9.7, and 13.0 lb/hr; carrier steam rates of 7, 14, 28, and 42 lb/hr; and column temperatures of 265, 300, and 315° F. Additional data have been obtained with a 4-foot packing height, using both 5 and 30 volume per cent TBP solutions, a solvent feed rate of 13.0 lb/hr, column operating temperature of 300° F, and carrier steam rates of 6.5 to 13.2 lb/hr.

The data for the 30 volume per cent TBP solutions, shown in Figure 1, indicate that the carrier-steam to solvent-feed weight ratio (SSR) required to limit the column bottoms (solvent residue) rate to approximately 1 per cent of the solvent feed rate increased from 2.2 to 3.9 when the packing height was decreased from 8 to 4 feet. The effect of a decrease in packing height from 8 to 4 feet varies from this nearly-doubled carrier steam requirement, at very low residue rates, to a negligible effect at residue rates greater than 20 per cent of the solvent feed rate.

Two runs were conducted using 5 volume per cent TBP solvent feed; one of these did not reach steady state conditions because of operational difficulties, and is, therefore, represented by a range of residue rates on Figure 2. The data obtained, however, were considered adequate for the intended purpose, and the run was not repeated. Figure 2 compares data obtained with a 4-foot packing height, a column temperature of 300° F, and using 5 and 30 volume per cent TBP-Amsco solvent feeds. The data show that a decrease in TBP concentration in the solvent feed decreases the steam-solvent ratio required to produce a given column residue rate. The limited data indicate that an SSR of less than 2 pounds of steam per pound of solvent would be sufficient to eliminate the bottoms stream with 5 per cent TBP-Amsco feed (for a 4-foot packing height at a column temperature of 300° F).

Results of a temperature profile taken with a 4-foot packing height are shown in Table 2. Since the solvent feed is not preheated, a portion of the packing is used to heat the feed. The data in Table 2 indicate that less than one foot of the packing was used to heat the solvent feed from room temperature to the vaporization temperature under the conditions employed.

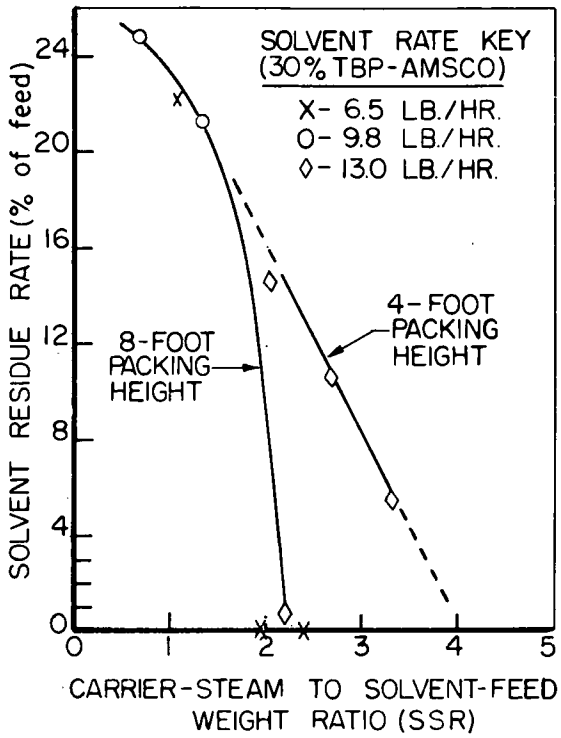

Fig. 1. Effect of Packing Height and Solvent-Steam Ratio on Solvent Residue Rate

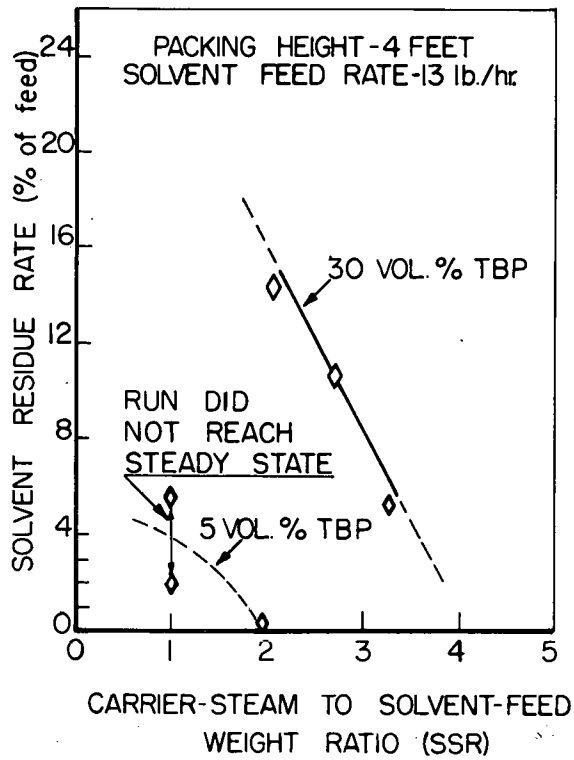

Fig. 2. Effect of TBP Concentration and Solvent-Steam Ratio on Solvent Residue Rate

Conditions: 4-inch diameter packed bed
1/2-inch Ceramic Raschig ring packing
Column temperature 300° C

TABLE 2

TEMPERATURE PROFILE IN PACKED BED

Conditions: (1) 4-inch diameter packed bed
(2) 1/2-inch diameter ceramic Rashig rings
(3) 4-foot packing height
(4) 30 volume per cent TBP-Amsco solvent feed
(5) Jacket temperature 304° F
(6) Solvent feed rate - 13.0 lb/hr

Run No.	Steam-Solvent Ratio (SSR) (lbs steam per lb solvent)	Bottoms Rate (per cent of solvent feed)	Temperature and Location (°F at indicated distance in inches from top of packing) 2	12	24	24*	36
14	2.0	14.6	241	296	294	296	304
15	2.7	10.8	251	292	291	293	304
16	3.3	5.4	260	292	291	294	303

* Located 1/4 inch from column wall; all others located on the axis of the column.

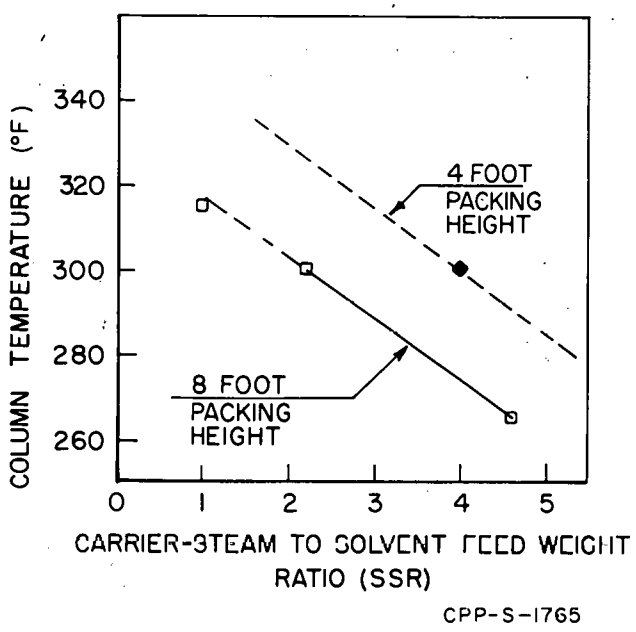

Conditions:

4-inch diameter packed bed
1/2-inch Ceramic Raschig ring packing
30 volume per cent TBP-Amsco feed
Zero column bottoms rate

Fig. 3. Solvent-Steam Ratio and Temperature Requirements for Elimination of Column Bottoms (Residue) Flow

Figure 3 shows an extrapolation of data to facilitate estimating the minimum carrier-steam to solvent-feed weight ratio (SSR) required to eliminate the bottoms stream for a given column temperature. The curve for an 8-foot packing height indicates that the variation with temperature is a straightline function over the range considered. By assuming that the lines representing 8-foot and 4-foot packing heights are parallel, it is possible to estimate the minimum SSR, at a given temperature, required to eliminate the bottoms stream, using a 4-foot packing height and a 30 volume per cent TBP-Amsco feed.

III. AQUEOUS PROCESSING STUDIES
Section Chief: K. L. Rohde, Process Chemistry

The process in use at the ICPP for recovering uranium from uranium-zirconium alloy fuels utilizes hydrofluoric acid as dissolvent and aluminum nitrate to complex the fluoride ion prior to solvent extraction. New processes are under development in an effort to reduce waste volumes, obtain less corrosive process streams, handle alloys of higher uranium content, and increase process equipment capacity.

The alloy fuels under consideration are 95 to 99 per cent zirconium; the extraction process capacity is limited by the requirement for handling this large volume of zirconium (a diluent of the uranium), and extraction raffinates generated involve an expensive storage problem because of the large volume and corrosive nature. In continuing studies directed at reduction of solution volumes to be processed, through separation of bulk zirconium from dissolver solutions, confirmation was made of a previous observation(1) that the use of a mixed precipitant (barium fluoride-barium nitrate) achieved more complete precipitation of zirconium and better separation of fission products than was obtained by the use of barium nitrate alone. Fission product zirconium and yttrium, as well as the previously-reported(1) strontium and cerium, were largely carried with the bulk zirconium precipitate, while niobium was found principally in solution with cesium and ruthenium.

In a study of alternate methods for separation of bulk zirconium, it has been found that the addition of sodium formate to zirconium-hydrofluoric acid dissolver solutions removes zirconium and fluoride almost quantitatively. Adjustment of the uranium to the VI oxidation state was necessary to avoid carrying uranium with the precipitate. Paraformaldehyde, formic acid, and salicylic acid were also investigated as zirconium precipitants, with less favorable results.

Results of a preliminary study on the recovery of uranium from a beryllia-uranium dioxide-containing ceramic fuel by a grinding-leaching technique are reported. Uranium has been extracted, by nitric acid leaching, from the pulverized ceramic material into solutions apparently suitable for solvent extraction, although optimum leaching conditions remain to be established.

A. Aqueous Zirconium Fuel Processing

1. Barium Fluozirconate Precipitation Process
J. W. Codding, Problem Leader; B. J. Newby

Scoping studies were continued in the last quarter to define fission product behavior during the precipitation of barium fluozirconate from STR dissolver solutions. Strontium, cesium, cerium, and ruthenium behavior was examined earlier under a variety of conditions(1). Because the radioactive solutions used had insufficient zirconium-95, niobium-95, and yttrium-91, these fission products have been studied separately. Their behavior has now been characterized during barium fluozirconate

precipitation from hydrofluoric acid-zirconium fluoride dissolver solution, using solid barium nitrate with and without solid barium fluoride as precipitants. Precipitations were carried out essentially as recommended in flowsheets prepared by B. E. Paige[2]. The effect of wash solution acidity was also scoped.

Experimental

Feed solution was prepared by adding tracers to radioactively cold, simulated STR dissolver solution. The latter was made by dissolving uranium-Zircaloy fuel in sufficient hydrofluoric acid to have a 5-to-1 mole ratio of fluoride to zirconium. Hydrogen peroxide was added to oxidize the uranium and to avoid precipitation of uranium tetrafluoride. Yttrium-91 was added as the oxide dissolved in 7M nitric acid; zirconium-95 and niobium-95 were added as oxalates dissolved in 0.5N oxalic acid. The final solution analyzed 1.45M zirconium, 1.45M nitric acid, and 7.3M fluoride. The zirconium-niobium tracer solution underwent a 1000-fold dilution upon addition to the dissolver solution. Under such conditions, the subsequent effect of oxalate would be negligible.

Equipment and procedures used were identical to those described for similar work reported in the previous Quarterly Progress Report[1].

Results

Macro zirconium, macro uranium, and fission product behaviors are summarized in Table 3 for several precipitation conditions. Precipitates formed using solid barium fluoride-barium nitrate as the precipitant carried almost 90 per cent of the zirconium-95, about 80 per cent of the yttrium-91, and approximately 5 per cent of the niobium-95. The fraction of zirconium-95 carried on the precipitates checked very closely with the fraction of macro zirconium found in the washed precipitate.

The use of solid barium nitrate alone resulted in less zirconium and yttrium-91, and more niobium-95, being carried by the precipitate. As was reported in previous work[1], this difference of fission product behavior between the two precipitants is the result of an incomplete reaction when using only solid barium nitrate; the inclusion of barium fluoride leads to a more complete precipitation.

Although 0.1N nitric acid was used as a precipitate wash in earlier process studies[2], 0.01N acid was recommended in order to minimize eventual acid addition to the supernate. The effect of wash acidity was accordingly examined in Runs 1 and 2. Table 3 shows that 0.01N acid was as effective as was 0.1N acid in removing uranium and inefficiently-carried fission products from the precipitate.

TABLE 3

FISSION PRODUCT BEHAVIOR DURING PRECIPITATION OF BARIUM FLUOZIRCONATE FROM STR DISSOLVER SOLUTIONS

(a) Using Solid Barium Nitrate with and without Solid Barium Fluoride as Precipitants

Run No.	Precipitation Techniques	Wash (d) Solution	Process Component	Material Distribution (Per cent by weight) Zr	U	Zr^{95}	Nb^{95}	Y^{91}
1	(b)	0.1N HNO_3	Filtrate	3.2	42	3.0	40	4.7
			Wash Solution	5.6	58	8.4	56	9.4
			Precipitate	91	0.4	89	3.6	86
2	(b)	0.01N HNO_3	Filtrate	2.7	27	4.9	23	7
			Wash Solution	8.7	72	7.2	69	18
			Precipitate	89	0.7	88	7.6	75
3	(c)	0.1N HNO_3	Filtrate	10.4	69	23	51	34
			Wash Solution	8.9	31	6	25	19
			Precipitate	81	0.1	71	24	47

(a) The dissolver solution composition was 1.5M Zr, 1.5N H+, and had a F^--Zr mole ratio of 5 to 1.

(b) 7.28g of solid BaF_2 and 10.8g of solid $Ba(NO_3)_2$ were added to 50ml. of dissolver solution; the slurry was stirred at 94° C for 2 hours.

(c) 21.8g of solid $Ba(NO_3)_2$ was added to 50ml. of dissolver solution; the slurry was stirred at 94° C for 2 hours.

(d) The residue was washed 4 times with 25ml. of HNO_3.

2. Additional Zirconium Precipitation Processes

J. W. Codding, Problem Leader; B. J. Newby

A scoping study was reported a year ago in which alternatives were sought to barium fluozirconate precipitation as a method for removing zirconium from hydrofluoric acid process solutions(3). Of the methods scoped, removing zirconium as a salicylate precipitate or as a hydrolysis product by boiling with paraformaldehyde and/or formic acid seemed to be the most attractive. These two methods have now been studied in more detail. A method which involves treating hydrofluoric acid dissolver solutions with sodium formate to remove zirconium as a hydrolysis product has also been examined in some detail and appears to be worthy of further study.

a. Zirconium Removal with Salicylic Acid

Several experiments were performed, attempting to remove zirconium from hydrofluoric acid process solutions, using salicylic acid as the precipitant after having first adjusted the solution to proper

acidity with nitric acid. The procedure described in earlier work on this subject was followed(3). Since the zirconium recovery realized in all experiments was less than 25 per cent, further work on this method was dropped.

b. Zirconium Removal with Paraformaldehyde and/or Formic Acid

Previous work(3) indicated that high zirconium recovery with small uranium losses could be accomplished by refluxing zirconium alloy-hydrofluoric acid process solutions with paraformaldehyde and formic acid for long periods of time. Since the hydrolysis product formed had a fluoride-to-zirconium ratio of about 3 to 1, the use of this method also resulted in the removal of large quantities of fluoride from the dissolver solution.

Because of the long refluxing times involved, attempts were made to speed up the reaction by refluxing simulated STR dissolver product solution with various amounts of paraformaldehyde and/or formic acid. The STR dissolver solution was prepared in the same manner and had about the same composition as a similar solution described in the previous section. Although the zirconium-containing solution was refluxed for as long as 6 hours with paraformaldehyde and/or formic acid, the best zirconium recovery obtained was about 80 per cent (see Table 4). Better zirconium recovery resulted from the use of formic acid or a combination of formic acid and paraformaldehyde than from the use of paraformaldehyde.

TABLE 4

ZIRCONIUM RECOVERY FROM SIMULATED STR DISSOLVER SOLUTION

(As a Function of Paraformaldehyde and/or Formic Acid Concentration after Six Hours of Total Reflux)

Moles of Formic Acid Used per Mole of Zr Involved	Moles of Paraformaldehyde (a) Used per Mole of Zr Involved	% Zr Removed from Dissolver Solution
	4.7	55
	7.1	60
	9.5	69
5		77
7.5		83
10		75
7.5	2.5	80
5	5	74
2.5	7.5	63

(a) The molecular weight of paraformaldehyde was assumed to be 30.

c. Zirconium Removal with Sodium Formate

It has been found that the addition of sodium formate to zirconium-hydrofluoric acid process solutions removes zirconium and fluoride almost quantitatively. Examination of the precipitates formed by X-ray failed to identify the material formed. Since the simulated process solutions from which the zirconium and fluoride were removed had a fluoride-to-zirconium mole ratio of 5 to 1, it was assumed that the same ratio would be found in the precipitates; this assumption was proved valid by zirconium and fluoride analyses. The addition of sodium formate probably causes a hydrolysis reaction; Blumenthal[4] states that sodium formate added to a zirconyl chloride solution results in the formation of a hydrolysate.

Effect of Sodium Formate Concentration

Zirconium recovery resulting from stirring uranium-Zircaloy dissolver solution for one hour with various concentrations of sodium formate at both room and elevated temperatures is shown in Figure 4. The preparation and composition of the dissolver solution used was almost identical to the solution described earlier. Sodium formate was added as a 26 weight per cent solution.

It is evident from the results that a sodium formate to zirconium mole ratio of two is adequate to assure maximum zirconium removal from solution.

The filtrate formed by adding sodium formate very slowly to a dissolver solution stirred either at 60° C or room temperature always contained a small amount of fine residue when allowed to stand for a short time. This can be prevented by adding the precipitant to a dissolver solution that is under total reflux or by treating at 60° C

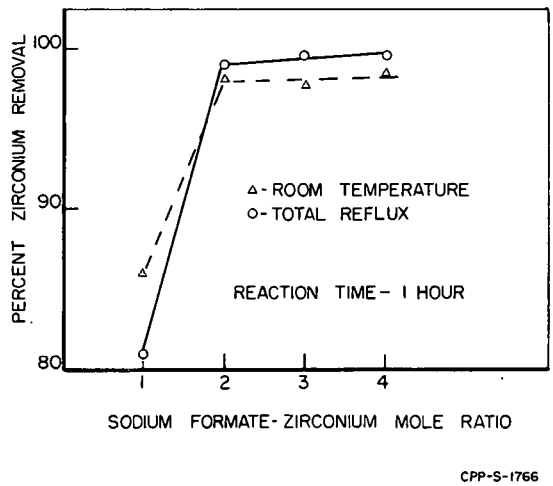

Fig. 4. Effect of Sodium Formate Concentration on Zirconium Recovery

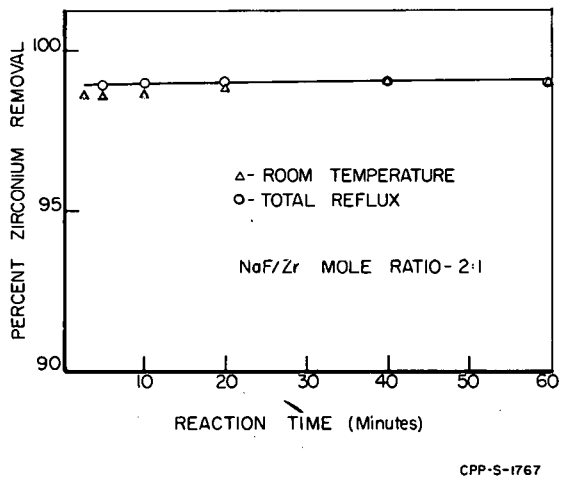

Fig. 5. Effect of Reaction Time on Zirconium Recovery

with flocculating agents after precipitant addition. Flocculating agents used successfully for this purpose were: potato starch, General Mills' Galactasol CAM, Dow's Separan NP10, and Stein Hall's Jaguar.

Effect of Reaction Time

At appropriate time intervals during a reaction between sodium formate and uranium-Zircaloy dissolver solution, at both room temperature and total reflux, aliquots of slurry were removed, filtered, and the filtrate analyzed for zirconium. The sodium formate-to-zirconium mole ratio was 2 to 1. These experiments showed (see Figure 5) that the precipitation reaction was very fast; it was complete within 5 minutes over the temperature range studied and was practically complete in 2-1/2 minutes.

Uranium Behavior

Water and 0.1M solutions of 9 different reagents were examined for their ability to remove uranium from the solid formed by sodium formate precipitation of zirconium at room temperature. Solutions tested were nitric acid, hydrofluoric acid, formic acid, sodium formate, sodium nitrate, sodium fluoride, ammonium nitrate, ammonium fluoride, and aluminum nitrate. Approximately 20g of residue were washed 4 times with 25 ml. of wash solution. The fraction by weight of residue dissolved by the wash solutions varied from 4.3 per cent for sodium formate and sodium nitrate to 13 per cent for nitric acid. At least 1/3 of this dissolved residue reprecipitated in the wash solution within a short time. About 20 per cent of the uranium originally found in the dissolver solution was held tightly by the residue and could not be washed off with any of the wash solutions. The uranium lost to the precipitate was reduced to 5 per cent by adding sodium formate solution (26 per cent by weight) very slowly to dissolver solutions stirred at 60° C followed by washing 4 times with 25ml. of 0.1N nitric acid.

Necessity for Uranium Adjustment

A further improvement was noted when no U^{IV} was present; when the above technique was preceded by boiling the dissolver solution with hydrogen peroxide to oxidize the uranium, the uranium loss was reduced to 0.1 per cent. The necessity of obtaining the uranyl species prior to precipitation is apparent.

Conclusions

The sodium formate method of zirconium and fluoride precipitation appears to be an attractive scheme for removing the bulk materials from STR-type dissolver solutions. Such removal should allow considerable concentration of the supernate for subsequent small volume solvent extraction processing, as well as providing greatly reduced waste volumes. Further studies of this system are planned.

B. Aqueous Ceramic Fuel Processing

1. Chemical Processing of $BeO-UO_2$, J. W. Codding, Problem Leader
L. A. Decker

A preliminary study is being conducted on the feasibility of a grind-leach flowsheet for chemical reprocessing of beryllia-uranium dioxide-containing ceramic fuels. The refractory, chemically-resistant nature of ceramic fuels requires drastic conditions to effect solution of the uranium content of the fuel.

Experimental

The fuel was ground in an Iler pulverizer, classified by passing through standard mesh screens, and separated into 5 groups: 10-20 mesh, 20-50 mesh, 50-100 mesh, 100-200 mesh, and less than 200 mesh. Three concentrations of nitric acid (3M, 6M, and 15.7M) were studied as possible leachants. Both stirred and non-stirred experiments were run, all at the boiling point of the solution. Single-stage leachings were conducted for periods ranging from 2 to 16 hours, while multiple-stage leachings were performed in successive steps, each of 1-1/2 hours' duration. After the leaching reaction, the material was filtered, washed with dilute nitric acid, and the supernate and wash solutions were analyzed for beryllium and uranium.

Results

Table 5 shows the results of scoping work done at two levels of acid concentration, two different leaching times, and two mesh sizes. No provision was made for stirring in this study. In general, long leaching times and high acidity were most effective in uranium recovery. It was noted, however, that the finer mesh powder was more difficult to leach with 3.0M acid, although this effect disappeared when using concentrated acid. It appeared that the action of two opposite effects might explain such behavior: as the particle size becomes smaller, greater specific area should increase the leach rate; but simultaneously, as particle size becomes very small, the formation and compaction in the grinder of powdered material inhibits leaching.

Accordingly, a series of experiments was done to determine the effect of particle size on the leach rate. Results are shown in Table 6 for constant acidity and leach time. It is noted that a maximum uranium recovery of 75 per cent occurs at an intermediate particle size; i.e., 100-200 mesh. The effect of stirring can also be noted when comparing Table 6 uranium recoveries for 20-50 mesh and -200 mesh sizes with the results shown in Table 5 for the same size ranges at 3.0M acid and 2-hour leach times; stirring markedly increases uranium recovery. This is especially evident in the case of -200 mesh material, the recovery increasing from 2.1 per cent, unstirred, to 67 per cent with stirring.

In an attempt to increase uranium recovery by successive leachings, experiments were run in which 100-200 mesh material was leached three successive times with nitric acid for 1-1/2 hours each;

TABLE 5

RECOVERY OF URANIUM FROM PULVERIZED CERAMIC FUEL
BY LEACHING WITH NITRIC ACID

(Boiling temperature, no stirring)

Original HNO_3 Concentration (M)	Leaching Time (hr)	Particle Size	Filtrate Concentration (g/l) Be Leach	Be Wash	U Leach	U Wash	Total Uranium Recovered %
3.0	2	20-50 Mesh	0.60	0.98	15.3	2.78	28
3.0	2	-200 Mesh	0.033	0.05	0.44	0.01	2.1
3.0	16	20-50 Mesh	3.6	0.2	32.6	2.13	72
3.0	16	-200 Mesh	0.28	0.06	3.86	1.32	14
15.7	2	20-50 Mesh	4.8	0.6	21.6	3.1	55
15.7	2	-200 Mesh	7.3	1.4	27.3	5.8	79
15.7	16	20-50 Mesh	19.5	2.1	32.2	3.2	76
15.7	16	-200 Mesh	21.8	4.5	26.3	4.8	72*

* Some material was lost during filtration; results expected to be low.

TABLE 6

RECOVERY OF URANIUM FROM PULVERIZED CERAMIC FUEL

Effect of Particle Size

(Boiling temperature, with stirring)
Leachant: 3M HNO_3
Leaching time: 2 hours

Particle Size	Filtrate Concentration (g/l) Be Leach	Be Wash	U Leach	U Wash	Total Uranium Recovered (%)
10-20 Mesh	0.31	0.01	4.6	0.2	36
20-50 Mesh	0.36	0.01	6.97	0.13	54
50-100 Mesh	0.61	0.02	8.82	0.25	71
100-200 Mesh	0.75	0.03	9.5	0.32	75
-200 Mesh	0.34	0.02	8.1	0.45	67

each filtrate was analyzed separately for uranium. The effect of acid concentration was also studied. Table 7 shows the results, confirming the earlier finding that recovery increases with acid concentration. The technique of successive leaching produced the greatest overall uranium recovery, namely, 80 per cent. However, this was only 5 per cent better than one 2-hour leaching and wash using 3.0M nitric acid.

Uranium concentrations as high as 32 grams/liter have been achieved; in the case of high-acid leaching, beryllium concentrations are in the same range. These solutions have been stable over several months. Such solutions should provide excellent feed for the solvent extraction recovery of uranium.

Work is continuing in an attempt to increase uranium recovery from the pulverized fuel.

TABLE 7

RECOVERY OF URANIUM FROM PULVERIZED CERAMIC FUEL BY SUCCESSIVE LEACHINGS

Effect of Nitric Acid Concentration

(Boiling temperature, with stirring)
Particle size: 100-200 mesh
Leaching time: 1-1/2 hours

HNO_3 Concentration (M)	Uranium Concentration in Filtrate (g/l) 1st Leach	2d Leach	3d Leach	Total Uranium Recovered (%)
3.0	7.56	1.32	0.05	67
6.0	8.97	1.32	0.08	77
15.7	9.29	1.35	0.19	80

IV. WASTE CALCINATION DEVELOPMENT AND DEMONSTRATION

Section Chiefs: J. I. Stevens, Waste Calcination Demonstration
J. A. Buckham, Technical Projects
D. W. Rhodes, Waste Treatment
R. A. McGuire, Pilot Plant Operations

Laboratory and pilot plant studies on the fluid bed calcination technique for reduction of aqueous aluminum nitrate waste solutions to solid alumina form have continued. The pilot plant two-foot-square calciner was operated to study the performance of individual feed spray nozzles designed for use in the Demonstrational Waste Calcining Facility in an effort to select a design offering maximum resistance to erosion in combination with reasonable control of the calciner operation. Flat-faced nozzles originally provided gave good operating control (presumably related to the spray pattern) but exhibited prohibitive erosion rates. A modified converging cone tip has been shown to have improved erosion resistance but to render process control more difficult by imposing greater restrictions on the operating range of nozzle air-to-liquid volume ratios.

Recent runs have indicated that the nitrate content and absolute density of the alumina produced in the pilot plant calciner are related to calcining temperature and/or feed composition as well as to alpha alumina content, as reported previously. Intra-particle porosity was also observed to vary with temperature and feed composition, but explanations for these observations have yet to be determined.

New and unexplained changes in the physical structure of the alumina produced during operation of the fluidized bed calciner have been observed. The last three runs made in the two-foot-square calciner have shown a rapid increase in the alpha alumina content of the bed (to a high of 36 to 48 per cent) during the first 6 to 18 hours of operation, followed by a gradual decline to a value between 4 and 12 per cent after 100 hours of operation. Previous observations were that if the alpha alumina content exceeded a value of approximately 28 per cent, the calcine bed was rapidly transformed to a bed containing over 60 per cent alpha alumina with no evidence of retrogression to a lower value.

Laboratory studies on the alumina structure indicate that it is influenced by a combination of variables including the presence of sodium nitrate and a variable atmosphere of air, water vapor, and oxides of nitrogen. Exposure of calcine samples to an electron beam in an electron microscope caused changes in the crystal structure within a few minutes.

Laboratory studies were continued on the calcination of acid waste solutions typical of those obtained from hydrofluoric acid dissolution of zirconium-based fuel. Calcination, without liberation of detectable fluoride, was accomplished after treatment with calcium oxide, giving promise to utilization of a stainless steel calcining system for treatment of zirconium fuel processing wastes.

Activities at the Demonstrational Waste Calcining Facility have been confined to functional testing of individual pieces of equipment and isolated process components, since construction additions and modifications were still being made. Results of erosion tests on proposed feed nozzles are given, and a possible method of process control, based on screen analysis of product, is discussed.

A. Research and Development in the Pilot Plant

1. Performance of Feed Nozzles in the Two-Foot-Square Calciner

E. S. Grimmett, Problem Leader; B. R. Wheeler, D. R. Evans
B. P. Brown

The two-foot-square calciner unit[5] was operated to study the performance of two feed nozzles designed as possible alternates to the Spraying Systems Company Type 1/2 J feed nozzles originally scheduled for installation in the Demonstrational Waste Calcining Facility (DWCF). During an earlier study[1], one of the original DWCF feed nozzles constructed of titanium, and a duplicate constructed of Type 347 stainless steel, were excessively eroded by the fluidized alumina in the two-foot-square calciner. The alternate feed nozzles tested in this study were constructed of Type 347 stainless steel, following designs indicated[1] to be less subject to erosion and differing from the Spraying Systems Company Type 1/2 J in the design of the nozzle air cap. Figure 6 compares the extended convergent and the extended divergent nozzle cap designs of the alternate nozzles used in this study with the Spraying Systems Company flat nozzle cap design originally specified for the DWCF nozzle. The alternate nozzles, although exhibiting improved erosion resistance, were found to have sufficiently peculiar atomizing characteristics to discourage further consideration.

The alternate nozzles were tested in two separate runs, for which pertinent calcining conditions are given in Table 8.

Run number 13, using the extended divergent nozzle, was terminated after only 6 days of operation because the alumina particle growth rate could not be controlled in the existing equipment; the particle size rapidly grew to a mass median particle diameter exceeding 1.2 mm, at which point poor heat transfer from the NaK tubes to the bed required run termination. Normally the particle size has been effectively controlled by changing the nozzle air-to-liquid volume ratio (NAR). A well-atomized spray has usually been produced with the Spraying Systems Company Type 1/2 J nozzle at an NAR of about 400; the average particle diameter of alumina generated at this NAR has been about 0.4 mm. During Run number 13, the NAR was raised to 1060 (by reducing the feed rate from 100 to 49 l/hr while increasing the atomizing air to a maximum) in a futile attempt to stem the particle growth in the bed. At run termination there was no evidence that the increase in NAR had any effect on particle growth; furthermore, numerous large agglomerates of particles had formed.

There are no plans for further performance studies using an extended divergent nozzle air cap on the Spraying Systems Company nozzle.

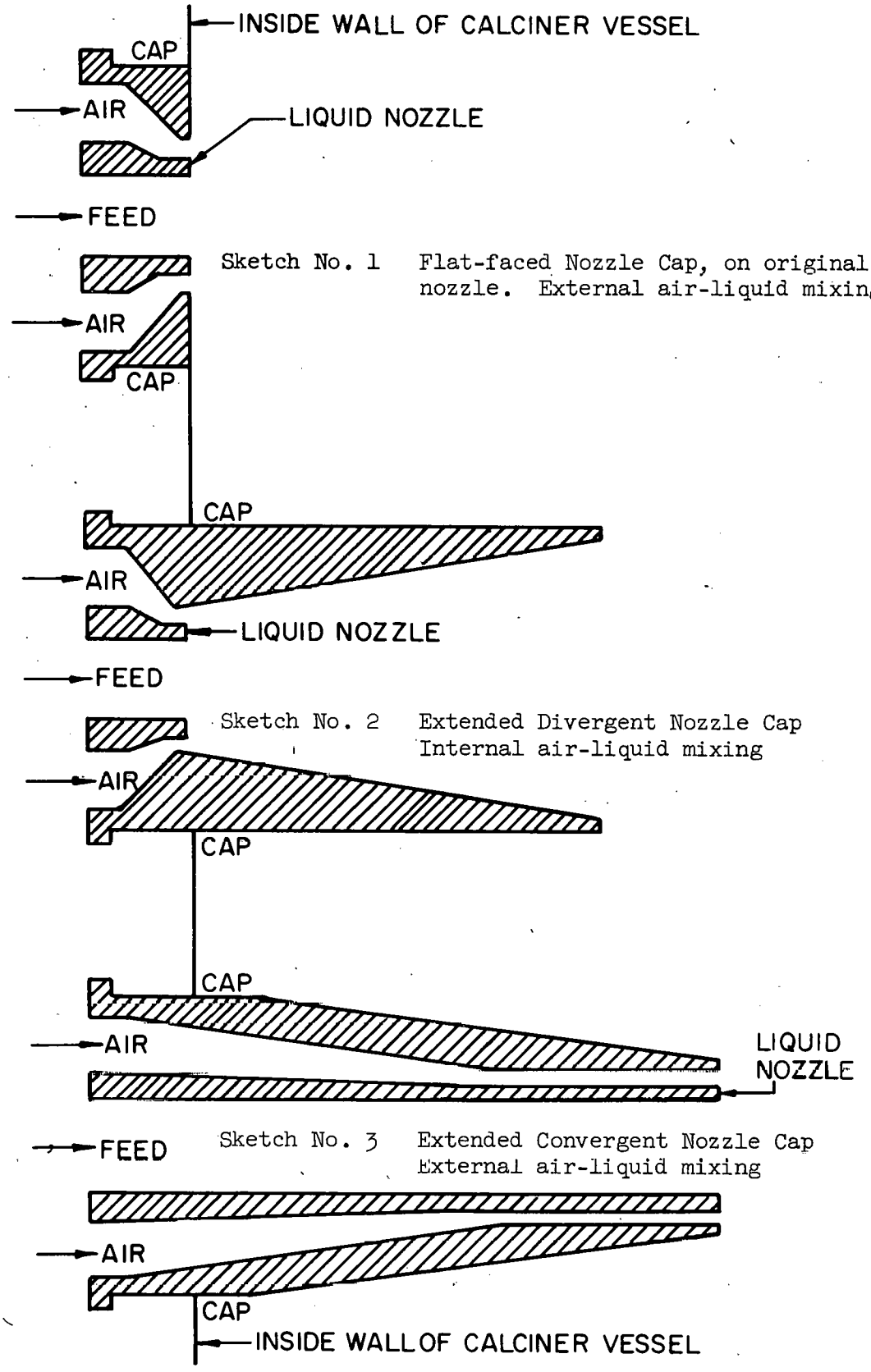

Fig. 6. Comparison of Various Nozzle Caps Used on Spraying Systems Company Type 1/2 J Nozzle in the Two-Foot-Square Calciner

TABLE 8

CALCINING CONDITIONS FOR THE PERFORMANCE STUDIES OF THE REDESIGNED DWCF FEED NOZZLES

	Run No. 13	Run No. 14
Number of nozzles	1	1
Nozzle cap	Extended divergent	Extended convergent
Nozzle sketch number on Figure 6	2	3
Bed temperature, °C	400	400
Nozzle air-to-liquid volume ratio (NAR)	Started at 400; increased to 1060	Various values between 250 and 400
Feed rate, l/hr	Started at 100, decreased to 49	Primarily 100; increased to 115 for about 70 hr
Superficial fluidizing gas velocity, ft/sec	1.0	1.0
Dry fines return	Below support plate	Partial return below support plate, until jet erosion which occurred on the 7th day of the 10-day run
Feed composition		
Aluminum nitrate $\underline{M}$	1.29	1.29
Nitric acid $\underline{M}$	2.84	2.84
Sodium nitrate $\underline{M}$	0.078	0.078
Mercuric nitrate $\underline{M}$	0.015	0.015

In order to use this nozzle cap, some auxiliary means of controlling particle size would apparently be required; for instance, a jet air stream could be employed to increase alumina attrition, thereby reducing the average bed particle size.

In Run number 14, a nozzle with an extended convergent nozzle air cap was tested. Various values of NAR between 250 and 400 were used in this run; data indicated that a value of NAR in the narrow range between 275 and 300 would be required to maintain the mass median particle diameter of the alumina product in the desired 0.3 to 0.6 mm range. Such an unusual sensitivity of product size to changes in NAR would be undesirable in an operating plant; therefore, any further testing of convergent nozzle caps would require a modified design. (During this run, the fines separated by the primary cyclone, and normally

returned to the bed, were periodically removed from the fines return system. If the dry fines return system had been operated continuously during the run, the numerical values of the limits of the operable NAR range would undoubtedly have been different; it is believed, however, that the operable range would still have been very narrow.)

In future runs, flat-faced nozzle caps of standard design will again be used, but they will be made of various materials harder than stainless steel to minimize the effects of erosion. Testing of nozzle caps of new design may also be resumed at a later date if promising designs are conceived.

2. Absolute Density and Nitrate Content of Alumina Produced in the Two-Foot-Square Calciner

It has been reported previously(6) that both absolute density and nitrate content were related to the alpha alumina content. The absolute density increases with increasing alpha alumina content, whereas the nitrate content decreases with increasing alpha alumina content. Additional data (from runs 13 and 14) corroborate the relationships; however, these properties now also appear to be somewhat dependent on calcining temperature and/or feed composition, as is shown in Figures 7 and 8.

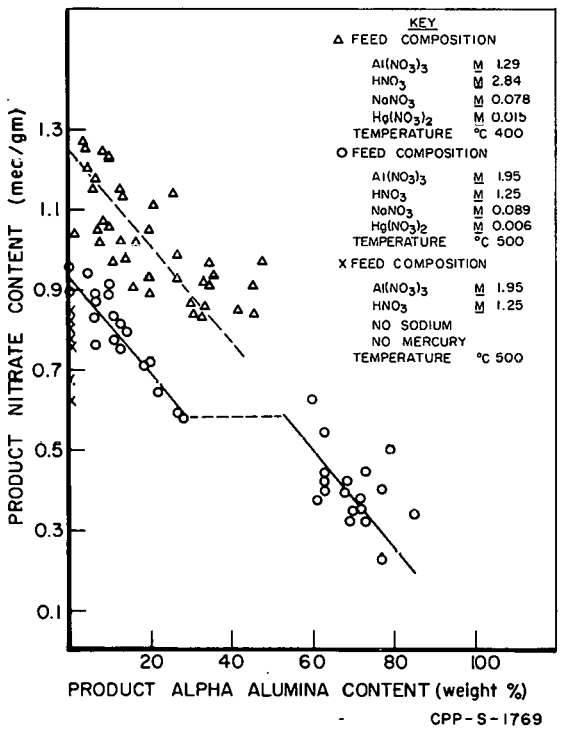

Fig. 7. Variation in Nitrate Content of Alumina Product

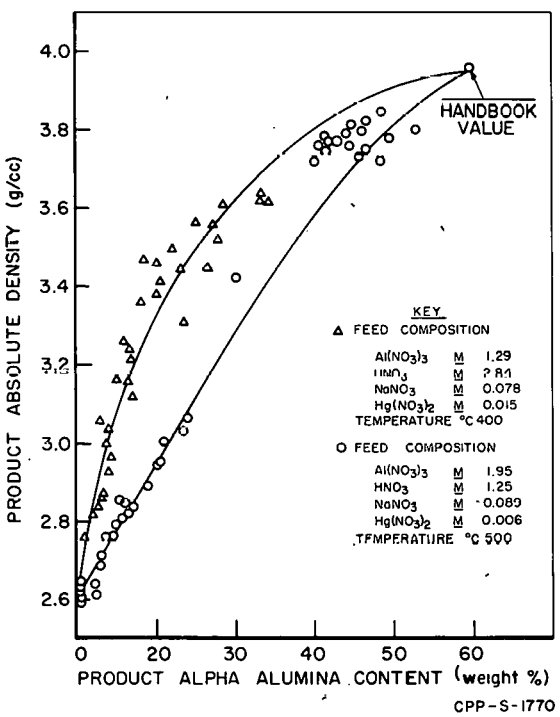

Fig. 8. Variation in Absolute Density of Alumina Product

The nitrate content of alumina generated at 500° C using a 1.95M aluminum nitrate solution is significantly lower than that of alumina (with similar alpha content) generated at 400° C using 1.29M aluminum nitrate solution. In independent experiments, the nitrate content of alumina has been significantly reduced by heating the alumina to temperatures higher than the generation temperature; therefore it is thought the difference in the nitrate content for the two sets of calcining conditions in Figure 7 is at least partially due to the difference in calcining temperature.

The nitrate in the alumina product is not necessarily in the form of sodium nitrate, in contrast to what might be assumed. Plotted to permit separate identification on Figure 7 are data representing analyses of alumina containing no sodium. The nitrate content of the alumina free of sodium was only slightly less than that of the sodium-containing, alpha alumina-free product obtained under similar calcining conditions. (No alpha alumina has ever been generated in the two-foot-square calciner when sodium has been completely absent from the feed solution.) Most of the sodium in the alumina is apparently in the form of an oxide.

The absolute density of alumina generated at 400° C using a 1.29M aluminum nitrate solution is higher than that of alumina of similar alpha content generated at 500° C using a 1.95M aluminum nitrate solution, as is shown by the data presented in Figure 8. This difference in absolute density is as yet unexplained, but it may be related to the difference in nitrate content.

3. Intra-Particle Porosity of Calcine

Recent determinations[1,6] of both the particle density and the absolute density of calcined alumina have made possible the calculation of the intra-particle porosity. (From a storage viewpoint, it is very desirable to generate alumina having a low intra-particle porosity.) Known porosities of alumina produced at 500° C using a 1.95M aluminum nitrate solution in the two-foot-square calciner have ranged between 0.52 and 0.66. During recent runs, when 1.29M aluminum nitrate solution has been calcined at 400° C, the porosity has ranged between 0.41 and 0.49. The cause of the low porosity has not been isolated; however, future runs in the two-foot-square calciner have been designed to do so.

4. Alpha Alumina Behavior in Calcine

Unique to the last 3 runs (Runs 12, 13, and 14) in the two-foot-square calciner has been a rapid increase in the alpha alumina content of the bed (from 12 per cent to a high of 36 to 48 per cent) during the first 6 to 18 hours of operation, followed by a gradual decline in alpha alumina content (to a value between 4 and 12 per cent) after 100 hours of operation. Figure 9 relates the alpha alumina content of the bed for each of these runs to the operating time after the aluminum nitrate feed solution was introduced to the calciner. (Equipment problems necessitated using a second bed after 32 hours of operation in Run 14; hence, two distinct sets of data points are shown from this run in Figure 9.)

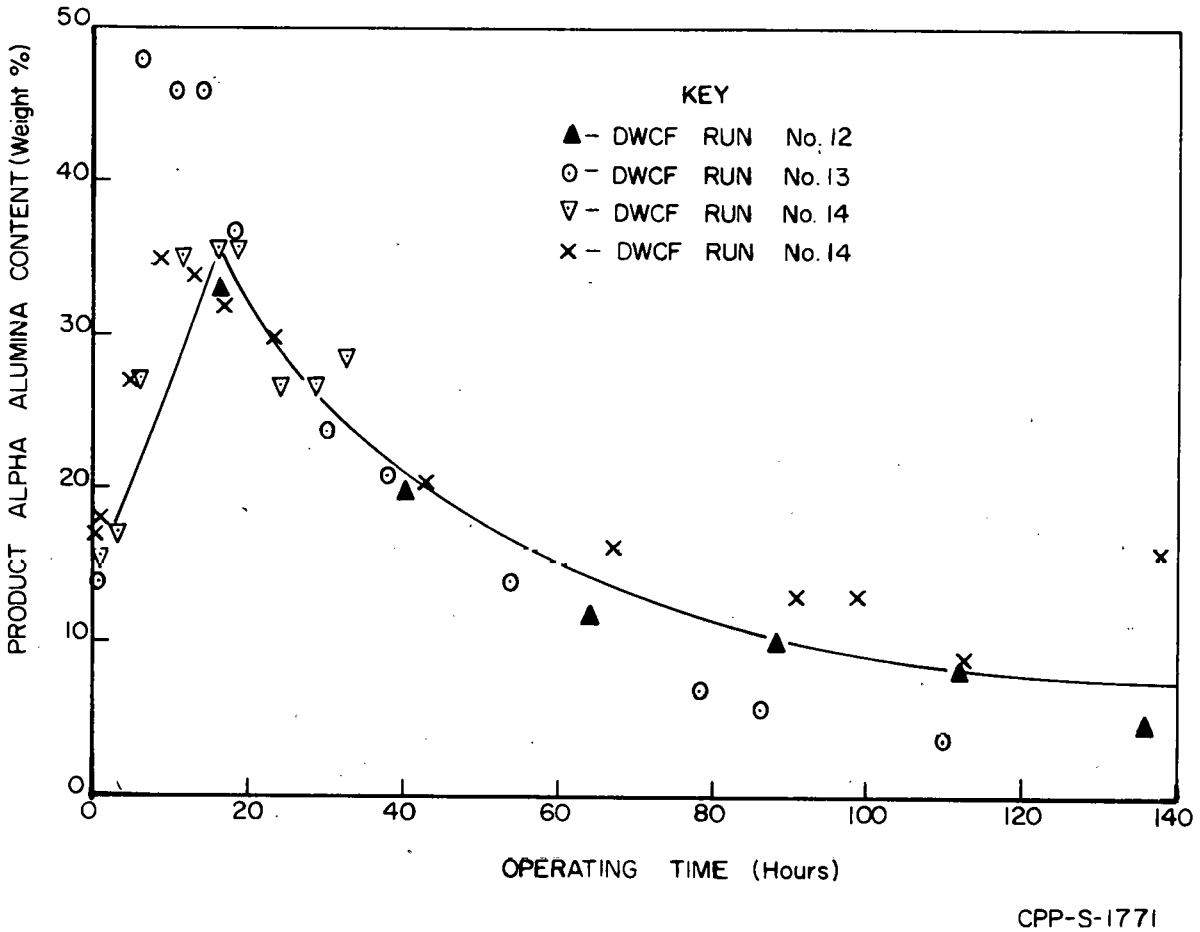

Fig. 9. Variation in Alpha Alumina Content of Alumina Product

The similarities in operating conditions on these three runs are given in Table 9. Other operating conditions -- such as feed rate, nozzle air-to-liquid volume ratio, type of nozzle cap, superficial fluidizing velocity, and dry fines return rate -- differed on these runs. (The data representing calcination at 400° C in Figures 7 and 8, which relate absolute density and nitrate content to the alpha alumina content, were obtained during these same three runs.)

The cause of this unique alpha behavior is not immediately apparent. In contrast to this phenomenon, during other calcination runs[6] at 500° C, beds having an alumina content slightly above 28 per cent were unstable and were transformed rapidly to beds containing over 60 per cent alpha alumina, with no evidence of any retrogression to a lower level alpha content prior to a change in calcining conditions. Future calciner runs will be designed to elucidate these phenomena.

TABLE 9

SIMILAR OPERATING CONDITIONS IN RUNS WHICH EXHIBITED EARLY PEAK IN PRODUCT ALPHA ALUMINA CONTENT

Bed temperature	400° C
Alumina for starting bed	Taken from product generated on Run number 11 during the period July 19 through July 27
Feed composition	
Aluminum nitrate M	1.29
Nitric acid M	2.84
Sodium nitrate M	0.078
Mercuric nitrate M	0.015

B. Laboratory Investigations

1. Calcination of Aluminum Nitrate Wastes

D. W. Rhodes, Problem Leader; R. F. Murray

The calcination of aluminum nitrate wastes in the pilot plant fluid bed calciner has produced either amorphous or alpha phase alumina or a mixture of both. To understand the causes of these phase changes more fully, experimental work was continued in the laboratory to evaluate the effects of the calciner system variables such as atmosphere, impurities, temperature, etc.

The primary purpose of the experimental work to date has been to determine the effects, if any, of the major variables in the system. Future experimental work is intended to define the kinetics and the mechanism of the phase changes to establish a sound theoretical basis for the phase change reactions, thus permitting the formation of any desired phase during calcination.

Heating amorphous calcined alumina in various atmospheres and with different added impurities in the 400 to 600° C range demonstrated that a combination of $NaNO_3$ plus an atmosphere containing air, water vapor, and the oxides of nitrogen markedly increased the rate of formation of alpha phase alumina. Under similar conditions, but without $NaNO_3$, a high proportion of gamma phase was formed.

Exposure of samples to the electron beam in an electron microscope caused some apparent changes in crystal structure within a few minutes.

Methods, Equipment, and Techniques

The experimental work in the laboratory was performed in a unit(*) holding three samples of calcined alumina and in which the atmosphere and temperature could be varied and different "impurities" combined with individual samples. The equipment was designed so that nitric acid dropped counter-current to a preheated air stream onto a porous plate. The decomposition products of the nitric acid circulated to the top of the furnace, then down through the screened sample holders containing the solid particles being tested. Thus far, all samples have been the same starting material, amorphous alumina from the pilot plant calciner. The samples were treated with various chemicals or different atmospheres, or both, and the phase changes noted.

Samples of the treated calcined alumina were examined by X-ray diffraction to determine the crystal phases present. To extend the range of data on phase formation available from X-ray diffraction, samples were examined by electron diffraction in the electron microscope at the University of Utah under the direction of Mr. N. L. Head. Small crystallite sizes (~ 20Å) produce diffraction patterns in the electron microscope, whereas X-ray diffraction shows an amorphous structure for crystallites of 100Å or less, even though a definite crystal phase may be present. In addition to the diffraction patterns, studies of the surface were made, and these gave some insight into the nature of particle formation.

Experimental Results

Samples of amorphous alumina prepared in the two-foot-square pilot plant calciner (product from April 13, 1960) were exposed to various atmospheres and temperatures under controlled conditions in the laboratory. Combinations of air, water vapor, nitric acid decomposition products, and mercury vapor were passed over the samples. The temperature ranged from 400 to 600° C. The data which are contained in Table 10 are grouped according to similarity of treatment, and the results are expressed in the amounts of a given phase found by X-ray diffraction following the indicated treatment.

These scoping studies show that certain factors in the system are very important. The combination that produced highest alpha content was $NaNO_3$ added to the amorphous alumina, followed by heating in a mixture of air and the decomposition products of HNO_3 (i.e., water vapor plus the oxides of nitrogen). In all samples heated in an atmosphere of air and water vapor, or air and nitric acid vapor, gamma alumina was formed. Samples without $NaNO_3$ consistently showed high amounts of gamma alumina with air and water vapor, or air and nitric acid vapors; however, water vapor and air produced the larger gamma crystals. Samples containing $NaNO_3$ exposed to the water vapor and air atmosphere produced less gamma alumina than those containing no $NaNO_3$; however, the presence of $NaNO_3$ resulted in the formation of an unidentified phase in addition to the gamma alumina.

(*) See IDO-14540 for a detailed description

TABLE 10

RESULTS OF EXPOSING AMORPHOUS ALUMINA TO NITRIC ACID, AIR AND WATER VAPOR AT ELEVATED TEMPERATURES

Sample No.	"Impurities" Added to Al_2O_3	Temp. °C	Conc. of HNO_3	Heating Time, Hrs.	Product (by X-ray) % α	% γ	Other
5A	None	500	0	954	<5	25	
3A	None	826	0	978	15	60	
2A	None	927	0	978	80	0	
53A	$NaNO_3$	500	6N	21	24	~20	$NaNO_3$
53B	$NaNO_3$	500	6N	69	35	~20	$NaNO_3$
54A	$NaNO_3$	500	6N	21	26	~20	$NaNO_3$
54B	$NaNO_3$	500	6N	69	32	~20	$NaNO_3$
65A	$NaNO_3$	500	6N	17	22	low	$NaNO_3$
65B	$NaNO_3$	500	6N	41	35	low	$NaNO_3$
65C	$NaNO_3$	500	6N	89	41	low	$NaNO_3$
65D	$NaNO_3$	500	6N	161	54	low	$NaNO_3$
67	$NaNO_3$	500	6N	42 (a)	53	low	$NaNO_3$
71	$NaNO_3$ (b)	500	6N	67.5 (b)	45	little	$NaNO_3$
55	$NaNO_3$	600	6N	72	25	~20	Unidentified
56	$NaNO_3$	600	6N	72	23	~20	Unidentified
57	$NaNO_3$	600	6N	72	21	~20	Unidentified
66A	None	500	6N	17	5	high	
66B	None	500	6N	41	5	high	
66C	None	500	6N	89	5	high	
78A	None	400	6N	21	0	low	
78B	None	400	6N	92	5	high	
78C	None	400	6N	163	7	high	
76A	$NaNO_3$	400	6N	21	29	low	$NaNO_3$
76B	$NaNO_3$	400	6N	92	39	low	$NaNO_3$
76C	$NaNO_3$	400	6N	163	43	low	$NaNO_3$
79A	$NaNO_3$	500	3N	18.5	40	low	$NaNO_3$
79B	$NaNO_3$	500	3N	90.5	57	low	$NaNO_3$
58	None	500	H_2O	69	6	~90	
59	None	500	H_2O	69	12	40-50	Unidentified

(a) Sample pretreated for 7 hours in air and water vapor, at 500° C, before addition of HNO_3.

(b) Mercury vapor present from 0.01M $Hg(NO_3)_2$ added to acid and sodium nitrate "impurity".

Although samples were heated at 400, 500, and 600° C under various conditions, no important differences were attributed to the effect of temperature.

Samples were pretreated for 7 hours in air and water vapor at 500° C and then HNO_3 was introduced into the furnace. Those samples which contained $NaNO_3$ showed an increased rate of alpha formation compared to those without the water vapor air pretreatment. The addition of Hg^{++} to the HNO_3 feed solution, so that Hg was vaporized at the calcination temperature, did not produce any change in the alpha formation rate, and similar results were also obtained when $Hg(NO_3)_2$ was added to the amorphous alumina. No important differences were noted in the rate of formation of alpha alumina using 3N or 6N nitric acid feed solution.

Some of the data are plotted in Figure 10 to demonstrate the differences between samples treated with $NaNO_3$ and those not so treated. The percentage of alpha alumina is shown as a function of time, and three temperature levels are noted. The only real differences are considered to be between the $NaNO_3$-treated samples and those not so treated.

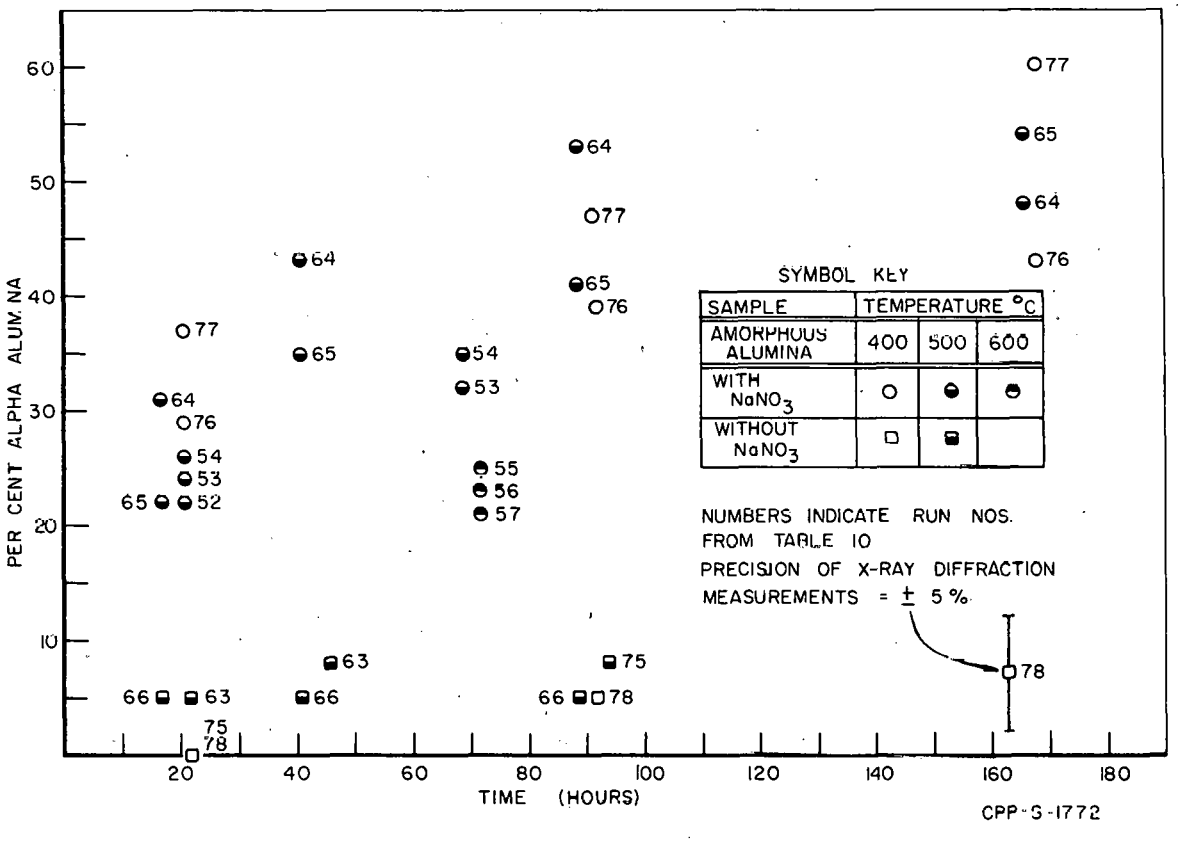

Fig. 10. Conversion of Amorphous Alumina to Alpha Alumina at 400-600° C

Some of the data plotted linearly in Figure 10 are replotted logarithmically in Figure 11. The percentage of alpha alumina approximates a slope of $(\text{time})^{1/3}$ where time is in hours. The line $10t^{1/3}$ has been drawn on the graph for comparison only, and is not intended to express an empirical rate law. As experimental work is completed, this rate correlation will receive more attention in an effort to determine what, if any, theoretical significance it may have.

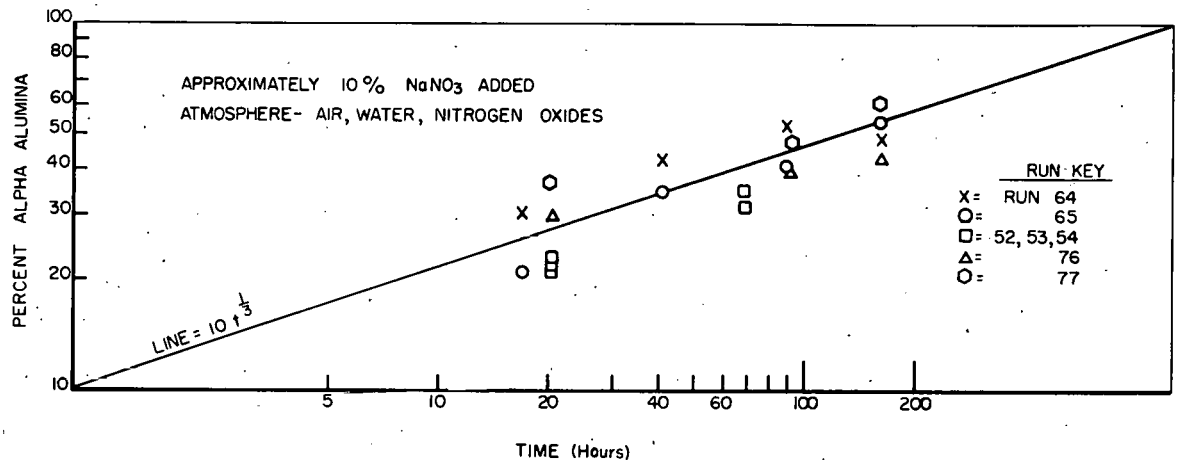

Fig. 11. Conversion of Amorphous Alumina to Alpha Alumina at 400-500° C (Logarithmic Plot)

Two samples of calcined alumina, which were amorphous by X-ray diffraction, were digested in 7M HNO_3, and the insoluble residue was examined by X-ray diffraction. The results are shown in Table 11.

TABLE 11

CRYSTAL COMPOSITION OF RESIDUES RESULTING FROM THE ACID DIGESTION OF AMORPHOUS (TO X-RAY) CALCINED ALUMINA

Exp. No.	Residue as % of Original Al_2O_3	Crystal Structure		
		γ Al_2O_3	α Al_2O_3	Other
1	66.2	30-40%	None	One or more unidentified species
2	18.3	80%	5%	

These data indicate that crystal phases are present even in the amorphous calcined alumina, but when present in small amounts, they do not give a characteristic X-ray diffraction pattern because of "masking" by the large quantity of material that is truly amorphous to X-rays.

Results of Electron Diffraction and Microscopy

Various samples of alumina prepared in the two-foot-square pilot plant calciner were examined in the electron microscope at the University of Utah, Salt Lake City, Utah. Diffraction patterns were made of all the samples, and surface replications at two magnifications were made of two of the samples. Mr. N. Lawrence Head operated the electron microscope and prepared or supervised the preparation of samples for examination.

The most outstanding feature of the examination was the gradual sharpening of the rings in some of the diffraction patterns during the electron bombardment, indicating that crystal growth was occurring. Examination of the photographs reveals this change, as noted in the captions for Figure 12 and Figure 13. Figures 14 to 17 consist of micrographs of surface replications of two samples at various powers of magnification. The amorphous sample in Figures 14 and 15 at 10^5 and 2×10^4 diameters respectively, shows an ordered arrangement of rounded particles in a series of parallel rows. Certain features of the pattern are worthy of note. Large particle size variations occur between rows, while there seems to be a relatively narrower range of particle sizes within a given row. The prominent line extending diagonally across the central portion of Figure 15 contains particles in the 250-500Å range in the upper portion of the line. Particles in the adjacent lines are in the 50-150 Å range. Other portions of the picture show a random orientation of particles. The matrix in which the particles are embedded appears quite smooth and shows no regular structural pattern. It may consist of a random orientation of small crystallites that have been laid down as a liquid and subsequently dried. The round particles which have already been dried may embed themselves in the still not-quite-crystallized layers formed by successive passes of the particle through the feed spray in the calciner.

The varied patterns seen, i.e., the layered regions and the regions of random scattering of particles on the surface, may represent different passes through the feed spray, with the large sphere of alumina growing in different directions each pass. Then the mechanical grinding action occurring while the material circulates through the bed may tend to smooth and round off the alumina spheres.

No great differences exist between the amorphous alumina (Figures 14 and 15) and the 90 per cent alpha alumina (Figures 16, 17). Two general observations may be made, however; the distinctive layer pattern appears more prominent in the amorphous alumina, although some order can be distinguished in the alpha alumina (Figure 16). Also, the base or matrix material is smoother in the amorphous than in the 90 per cent alpha alumina.

This first attempt at examination of the micro structure of calcined alumina by electron diffraction and microscopy suggests that further work along this line should be undertaken. Measurements of the spacings should be made to identify the phases, and the effect of irradiation on crystal growth needs evaluation. In addition, more

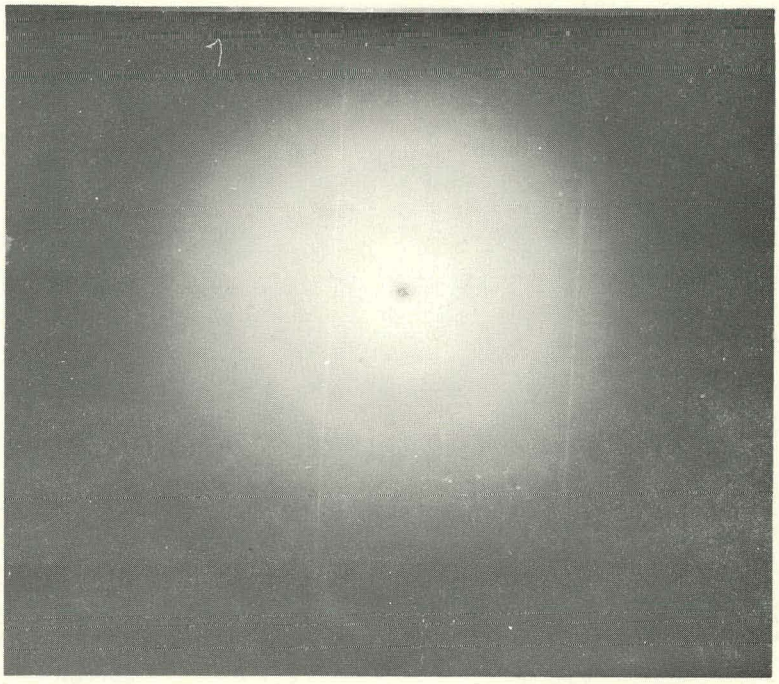

Fig. 12. Electron Diffraction Pattern of Amorphous (to X-ray) Alumina

Fig. 13. Same as Fig. 12, After Four-Minute Exposure to 40 Kv Electrons

Fig. 14. Amorphous Alumina
Magnification 100,000

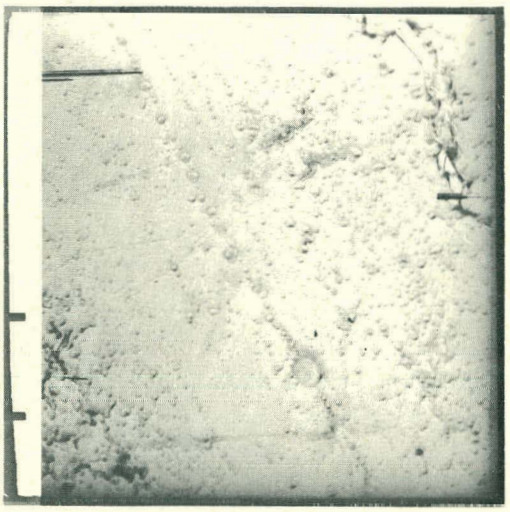

Fig. 15. Same as Fig. 14
Magnification 20,000

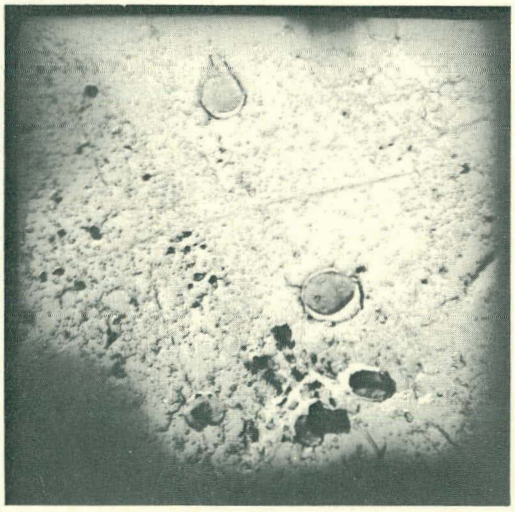

Fig. 16. 90% Alpha Alumina
Magnification 38,000

Fig. 17. Same as Fig. 16
Magnification 10,000

surface photomicrographs should be made to help explain more fully the mechanics of particle formation.

2. Calcination of Zirconium Fluoride Wastes

D. W. Rhodes, Problem Leader; J. S. Madachy

Laboratory research was continued to determine the optimum temperature for the calcination of acidic waste solutions containing, as major chemical components, zirconium, aluminum, fluoride, and nitrate. The proposed method involves precipitation of the zirconium, fluoride, and much of the aluminum by the addition of calcium oxide and calcination of the resulting slurry.

Calcination at 400, 435, 465, 500, and 535° C indicated that no detectable amount (less than 0.25 per cent) of the total fluoride was volatilized and collected in the caustic scrubbers. Leachability of the residue in water at 25° C decreased from 11 per cent to 2 per cent over the temperature range, and the ratio of calcium to fluoride in the leachate also decreased with increasing temperature, suggesting that at the higher temperatures the soluble material was largely calcium fluoride, while at the lower temperatures there was also some unreacted calcium oxide which dissolved.

Methods and Materials

The precipitation and calcination steps were carried out in a small laboratory calciner as described in a previous report(1). The synthetic zirconium waste solution contained 0.52M zirconium, 0.55M aluminum, 2.84M fluoride, 1.65M nitrate, and 0.685M hydrogen ion. The amount of calcium which was added, as calcium oxide, to the waste solution, was in all cases chemically equivalent to the amount of fluoride present. To prepare the waste for calcination, the calcium oxide was added to the waste solution, the slurry stirred for two hours, and then allowed to stand overnight prior to calcination. Calcination temperatures investigated were 400, 435, 465, 500, and 535° C.

Leachability of the calcined residue was determined by stirring a 0.3 gram sample in 100 ml of water for 24 hours at room temperature. The undissolved residue was filtered, dried, and weighed. Samples of the calcined residue, scrubber solutions, and leachates were analyzed for fluoride, zirconium, calcium, and pH.

Experimental Results

X-ray diffraction analysis of the calcined residues indicated that calcium fluoride and zirconium oxide were the only crystalline components present. No unidentified crystalline components were found.

The results of the calcination experiments are summarized in Table 12.

TABLE 12

RESULTS OF CALCINATION OF SYNTHETIC PROCESS WASTES CONTAINING ZIRCONIUM FLUORIDE

Calcination Temperature °C	Fluoride in Absorbers (% of total)	Residue Leached by Water (wt. %)	Composition of Leachate µg/ml of: pH	Ca	F	Zr	Ca/F (wt.ratio)
400	<0.25	11.05	8	58	13	<5	4.5
400	<0.25						
400	<0.25	7.69	8.2	48	14	<5	3.4
435	<0.25	9.81	8.2	8.2	68	<2	13.5
435	<0.25	5.86	8.2	52	13	<2	4
465		2.74	7.3	15	16	<4	0.94
465	<0.25						
465		2.41	7.1	11	13	<4	0.85
500	<0.25	2.59	7.6	37	16	<2	2.5
535		1.69	6.8	8	9	<4	0.89

In all cases, the amount of fluoride in the scrubber solution was below the detectable limit; however, analysis of the calcined residue indicated an apparent loss of fluoride of 2 to 17 per cent. It is not yet known whether this low material balance is real, or due to difficulties in determining fluoride accurately in the calcined residue. Based on the preceding data, the choice of a calcination temperature between 400 and 535° C would be determined primarily by the need to produce a highly insoluble residue, inasmuch as fluoride volatility did not appear to be a function of temperature within the range studied.

C. Demonstrational Waste Calcining Facility
Section Chief: J. I. Stevens

1. Program Planning and Data Correlation
B. M. Legler, Problem Leader; G. E. Lohse

2. Technical Surveillance, L. T. Lakey, Problem Leader
E. J Bailey, P. N. Kelly, J. L. Lockard, E. A. Travnicek

Beneficial occupancy of the major portion of the Demonstrational Waste Calcining Facility was obtained during this period. Functional tests of equipment were continued, and isolated process component tests were begun.

Construction Additions and Modifications

As a result of continued checking of designs as well as findings of preliminary functional tests, the additions and modifications to the Demonstrational Waste Calcining Facility approved during this period include (1) a second NaK expansion tank, and (2) revised liquid piping and control valving in the quench and venturi scrubber system.

Functional Testing of Equipment

Equipment and process checkouts of the facility were continued during this period. It was impossible to attain an integrated process system for testing because of various deficiencies. Major deficiencies that prevented process testing were overheating of bearings in the off gas blowers and vibration in the solids transport air blower(7). Replacing the silicone-base grease with one manufactured from an edible beef tallow base (Lubriko-M-24, manufactured by Masters Lubricant, Inc.) recommended by the blower manufacturer, plus alignment in the thermally hot condition, has markedly improved blower operation. The vibrational problem in one of the transport air blowers, however, has not been resolved, and it is suspected that the blower shaft may be bent. Further checking is necessary to determine if this condition exists.

The ruthenium adsorbers have been charged with silica gel. Testing of the regeneration cycle and equipment was started on one of the adsorbers. Saturation of its silica gel with water was completed. It was found that the silica gel did not decrepitate when contacted with liquid water if its moisture content was above 34 weight per cent on a dry basis. This compares favorably with small scale tests by the architect-engineer which established 38 weight per cent as the probable degree of saturation required. Completion of the regeneration cycle (flooding with water, followed by drying) awaits return of the off gas blowers to service. Damage from freezing of the coils in the heating and ventilating system must be corrected before further regeneration tests can be made, since heating of the adsorber cells is required to prevent condensation in the vessels.

The calciner feed hopper was filled with alumina produced at the Cold Pilot Plant in the two-foot square calciner and stockpiled in anticipation of cold runs in the DWCF. The Johnston deep-well-type pumps were installed temporarily to permit checkout of the quench system while awaiting delivery of the Lawrence pumps which will replace them.

Leaking NaK dump valves were repaired, and the NaK charge for the heat transfer system was put into the drain and charge tanks. The NaK loop was filled by pressuring from these tanks. After filling of the loop, the NaK furnace was fired successfully for a short period at a low rate.

Feed Nozzle Testing

The severe erosion of titanium and Type 347 stainless steel flat-faced nozzle tips of the Spraying Systems Company Type 1/2-J pneumatic atomizing nozzles used in cold pilot plant calciner runs has

necessitated a test program to determine if a better design, a better material of construction, or a combination of both could be found. Results of erosion tests previously reported[1] indicated that extended converging or diverging cone tips were eroded at substantially reduced rates.

Tips of these designs were fabricated of Type 347 stainless steel and used during regular 400° C runs of the two-foot square Cold Pilot Plant calciner. To obtain more accurate estimates of erosion rates, the tip weight losses recorded for each run were reduced to a volumetric loss rate (in^3/yr), since the effect on nozzle performance is dependent primarily on volume of metal eroded at the face of the air nozzle.

Results of the tests are summarized in Table 13. The best performance, based on a minimum volume loss rate, was achieved with the extended converging cone tip. This design has a disadvantage, however, in that an alteration of the nozzle cleanout plunger and bellows assembly is required for use in the DWCF. The investigation will be continued with hardened, flat-faced nozzles and modified cone tips.

TABLE 13

FEED NOZZLE TIP EROSION RESULTS

Nozzle Designation (a)	Hours Tested	Wt. Loss Grams	Vol. Loss Rate in^3/yr	Remarks
SS-347 22° Diverging Cone	138.5	0.0456	0.02225	Erosion occurred over entire inside surface of cone.
SS-347 22° Converging Cone	169	0.0049	0.00157	

(a) Details of nozzle tip designs are given in third quarterly, (IDO-14540)

Product Quality Control

After the Demonstrational Waste Calcining Facility goes "hot", it will be imperative that the operation be under control at all times. The most direct indicator of process trend is product quality. Present analytical data obtained in the Cold Pilot Plant to define product quality, i.e., mean particle diameter, bulk density, alpha content, attrition index, etc., would be difficult to obtain on a radioactive product. There is, however, a good possibility of making a single screening cut on this material, i.e., measurement of retention on a particular screen size, if it can be shown to be a valid indicator for process control. Consequently, a review of data from pilot plant runs was undertaken. A limited amount of data has been reviewed, but definite conclusions cannot yet be drawn; however, the data show sufficient promise to warrant continued study.

V. NEW WASTE TREATMENT METHODS

Section Chief: D. W. Rhodes

The long-range program in radioactive waste management at the ICPP aims to reduce waste volumes to a minimum, store wastes as non-leachable solids, separate the non-radioactive alloy components from the fission products, and follow tank corrosion where liquid wastes are stored in temporary tanks. Toward these goals, results are presented on the specific removal of cesium and strontium from gross waste by adsorption on ammonium phosphomolybdate and resins, respectively, and on the process chemistry of the mercury cathode removal of iron, nickel, and chromium from stainless steel wastes.

A. Removal of Long-Lived Radioisotopes from Waste Solutions

M. W. Wilding

Research on the removal of long-lived radioisotopes from synthetic waste solutions consisted of additional studies of the removal of cesium from synthetic ICPP waste by adsorption on ammonium phosphomolybdate (APM) and removal of strontium from acidic solutions by the use of ion exchange resins. Investigation of the removal of cesium from synthetic ICPP waste as a function of concentration of cesium indicated that the average distribution coefficient (K_d) for cesium varied less than 10 per cent from 3600 when the concentration of cesium in the waste solution was between tracer concentrations and 0.068 grams of cesium per liter, the approximate ICPP waste concentration. At concentrations greater than 0.068 grams per liter, K_d decreased rapidly to a value of about 3 at 68 grams of Cs per liter of waste. At the lower concentrations, ion exchange appeared to be the predominant mechanism, but above 6.8 grams of cesium per liter, another reaction -- probably precipitation -- also functioned in the removal of cesium from solution.

Batch equilibrium experiments with three Amberlite organic ion exchange resins indicated that distribution coefficients for strontium in 0.1N nitric acid without interfering salt ions present exceeded 1000. In the presence of 1M aluminum nitrate, however, the distribution coefficient for strontium was reduced to about 66 for the Amberlite 200, the only resin tested under these conditions.

Methods and Materials

Batch equilibrium experiments for determining the effect of cesium concentration on the removal of cesium from synthetic ICPP waste solution consisted of contacting one gram of APM for 36 hours with 20 milliliters of a solution containing 1N nitric acid, 2M aluminum nitrate, and various concentrations of cesium nitrate traced with cesium-137.

Experiments to measure the extent of removal of strontium from solution consisted of batch equilibrium experiments with 20 milliliters of a solution containing 0.02 grams of strontium (traced with strontium-85) per liter of 1N or 0.1N nitric acid and 2 grams (dry weight) of organic resin. The organic resins were Amberlite IR 120 and Amberlite IR 122 --

nuclear sulfonic-acid types -- and Amberlite 200, a sulfonated styrene-divinyl-benzene copolymer type.

Experimental Results

The distribution of cesium between the synthetic waste solution and the solid APM is shown in Figure 18 and Table 14.

TABLE 14

ADSORPTION OF CESIUM BY APM FROM SYNTHETIC ICPP WASTE AT 25° C

Concentration of Cesium in Waste mg Cs/ml Solution	Equilibrium Concentration of Cesium		Distribution Coefficient K_d
	mg Cs/g APM	mg Cs/ml Solution	
1.6×10^{-8}	3.2×10^{-7}	0.9×10^{-11}	3660
3.4×10^{-3}	0.07	1.9×10^{-5}	3620
6.8×10^{-3}	0.14	3.8×10^{-5}	3600
0.017	0.34	9.4×10^{-5}	3590
0.034	0.68	1.9×10^{-4}	3490
0.068	1.35	4.1×10^{-4}	3310
0.17	3.38	1.2×10^{-3}	2770
0.34	6.74	2.5×10^{-3}	2210
0.51	10.1	6.2×10^{-3}	1630
0.68	13.4	0.012	1240
3.4	36.7	1.6	23.5
6.8	48.4	4.4	11.0
17.0	71.0	13.4	5.3
34.0	104.0	28.8	3.6
68.0	190.0	58.5	3.3

The data in Table 14 and the shape of the curve in Figure 18 suggest that ion exchange is the predominant mechanism resulting in the removal of cesium from a synthetic waste having the approximate chemical composition of ICPP waste and a concentration of less than 6.8 grams of cesium per liter. Above 6.8 grams per liter, a secondary mechanism -- probably precipitation -- also appears to be functioning. The ICPP aluminum nitrate-nitric acid wastes in storage contain approximately 0.06 grams of cesium per liter, which is well within the range for ion exchange to predominate. A small scale experiment using APM in a fixed bed column and first cycle process waste will be needed to evaluate the effectiveness of this process for removing cesium from acidic high-level wastes.

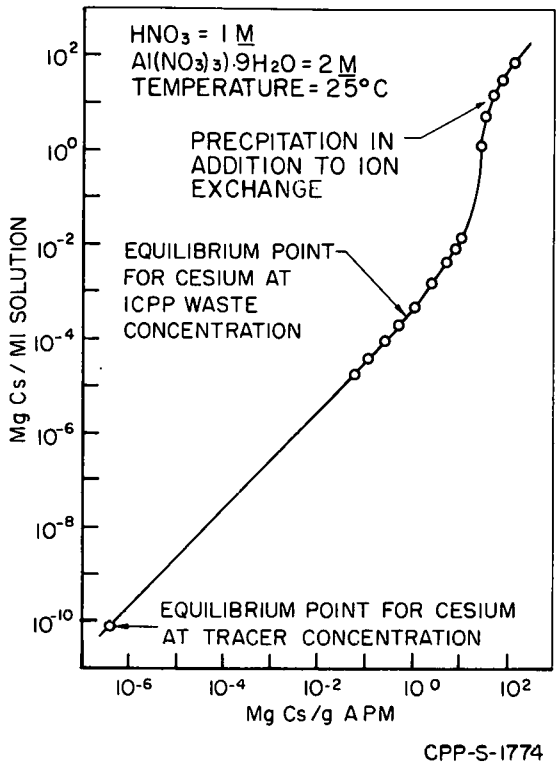

Fig. 18. Equilibrium Distribution for Cesium in Synthetic ICPP Waste

The results of equilibrium experiments to measure the removal of strontium from acidic solutions by adsorption on organic ion exchange resins at two different concentrations of nitric acid are shown in Table 15. The Amberlite 200 resin appeared to be the most effective of the three resins tested for the removal of strontium from acidic solutions. The addition of sufficient aluminum nitrate to the 0.1N nitric acid to make the solution 1M aluminum nitrate reduced the distribution coefficient to 66. Additional experiments with Amberlite 200 in 0.1N hydrochloric, sulfuric, and hydrofluoric acids containing 0.02 grams per liter of strontium traced with strontium-85 gave distribution coefficients greater than 8×10^3. No visual breakdown of the resins occurred in the acid solutions, but additional testing will be required to evaluate possible effects on the exchange capacity.

TABLE 15

ADSORPTION OF STRONTIUM FROM ACIDIC SOLUTIONS BY ION EXCHANGE RESINS AT 25° C

Resin	Equilibrium Distribution Coefficient in: 1N Nitric Acid	0.1N Nitric Acid
Amberlite IR 120	105	1230
Amberlite IR 122	134	4000
Amberlite 200	300	6900

B. Mercury Cathode Electrolysis of Stainless Steel Wastes
D. R. Anderson

Laboratory study was continued on the removal of the alloy metal ions (iron, nickel, and chromium) from synthetic stainless steel process

wastes by mercury cathode electrolysis. Data obtained previously[1,6,8] indicated that mercury cathode electrolysis could be used to effect a separation of the alloy metal ions from essentially all of the fission products except zirconium and possibly ruthenium.

Current laboratory data indicate that at -1.80 volts vs S.C.E. and at room temperature, the maximum rate of removal of the alloy metal ions from the synthetic waste was obtained in solutions of greater than 2N or less than 0.5N sulfuric acid. The slowest removal occurred in 1N sulfuric acid. At solution temperatures above 35° C, the apparent inhibiting effect of 1N sulfuric acid on the removal of the alloy metal ions was eliminated.

The results of experiments in which alloy metals were electrolyzed until solidification of the amalgam occurred indicated that the mercury could contain approximately 2 per cent by weight of stainless steel alloy metal ions and still retain its fluid properties.

Experimental Methods and Equipment

Preparation of the amalgams containing stainless steel metal ions for investigation of the physical characteristics was performed in a Bolger electrolysis vessel[1]. About 200 ml of a solution of the sulfate salts were placed in the cell over a 15 to 20 ml pool of mercury. The anode was a 1-inch diameter platinum screen. The mercury-aqueous interface was stirred continuously, and a battery charger was used to supply 6 volts DC to the cell. The temperature of the solution, which was not controlled during electrolysis, rose to 40° C and higher on occasion.

The alloy metal ion removal rates were determined by electrolysis of synthetic waste solutions in a conventional Dyna-Cath mercury cathode electrolysis analyzer. The applied potential was maintained at -1.80 volts vs S.C.E., the potential below which fission products were not reduced, and aliquots of the waste solution were removed periodically to determine the completeness of the electrolysis. The temperature was controlled in the 25° to 40° C temperature range by means of a thermoregulator assembly and associated water bath. For measurements above 40° C, the solutions were allowed to self-heat without cooling.

Experimental Results

Amalgams containing about 1 per cent by weight each of iron and nickel and 0.1 per cent by weight of chromium were formed in the Bolger cell, using a 2N sulfuric acid solution containing equal concentrations (~ 0.15M) of each of the alloy metal ions, without causing the amalgam to lose its fluid properties. Preparation of amalgams from 0.2N sulfuric acid solutions containing alloy metal ions in approximately waste concentrations (0.1M iron, 0.02M chromium, and 0.01M nickel) indicated that an amalgam containing approximately 2 weight per cent of metal ions could be prepared without causing the amalgam to lose its fluid properties. These data are largely qualitative, but do indicate to some extent the concentration of amalgams which might be prepared under process conditions. For process design purposes, it will be necessary to make

detailed measurements of the viscosity of the amalgams as a function of metal alloy concentration.

In the Dyna-Cath equipment, short-circuiting of the electrical system in the cell by amalgam growth from the cathode to the anode occurred at a loading of less than 2 per cent deposited metals. Elimination of this difficulty is possible by suitable design of the cell equipment. For example, similar difficulties were overcome in the removal of nickel from HRT fuel solutions by mercury cathode electrolysis by introducing a stream of fuel solution under the mercury cathode to provide agitation(9).

At room temperature, the rate of removal of the alloy metals was sensitive to the initial concentration of sulfuric acid in the solution. For example, Figure 19 indicates complete removal of the alloy metal ions at low and high acid concentrations in 80 amp-hr and at a potential of -1.80 volts vs S.C.E., whereas an initial acid concentration of about 1.0N H_2SO_4 resulted in removal of only about 26 to 84 per cent of the alloy metal ions under the same cell conditions.

Increasing the temperature of the waste solution to 35 degrees or above markedly increased the removal rate of all three metals in a solution of 1N H_2SO_4. Figure 20 indicates essentially complete removal of all three of the stainless steel metal ions from 1N H_2SO_4 solution in 30 amp-hr at 35° C, whereas removal of all three metals was incomplete in 80 amp-hr at room temperature (Figure 19).

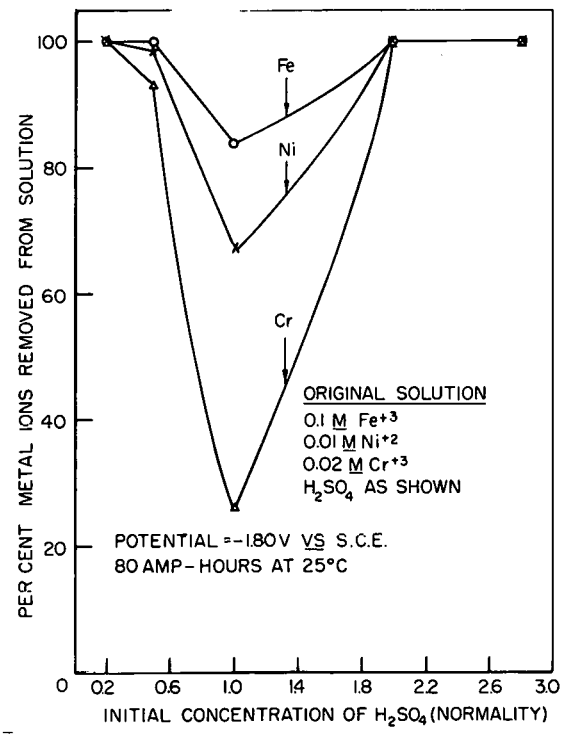

Fig. 19. Removal of Stainless Steel Metal Ions from Synthetic Waste Solution at 25° C as a Function of Initial Sulfuric Acid Concentration

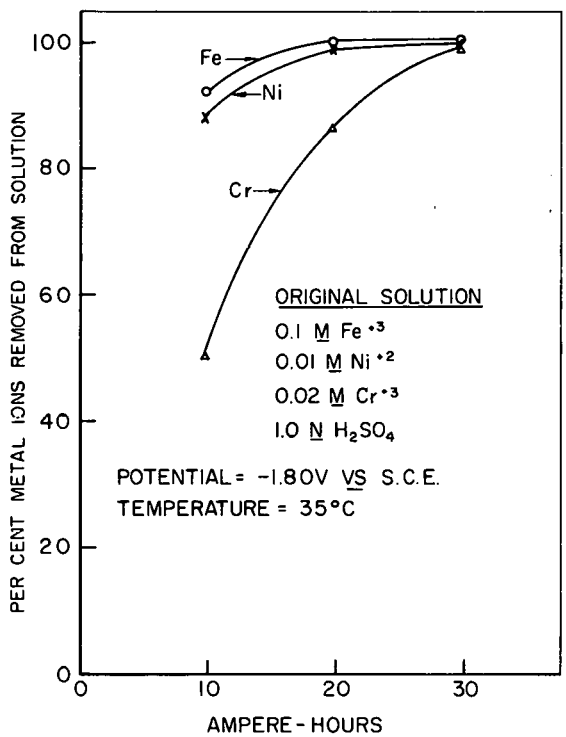

Fig. 20. Removal of Stainless Steel Metal Ions from Synthetic Waste Solution at 35° C as a Function of Ampere-Hours

Research has not yet been initiated with the specific objective of determining why sulfuric acid concentration and temperature affect the alloy metal ion removal rate, but an understanding of these phenomena will be necessary for the successful development of a waste treatment process. Qualitative observations suggest that the chromium ion has an apparent inhibiting effect on the removal of iron and nickel, and that the ion species in solution and the characteristics of the amalgams undoubtedly influence the electrolysis reaction.

VI. ELECTROLYTIC DISSOLUTION SYSTEMS

Section Chiefs: H. T. Hahn, Chemical Research
K.L. Rohde, Process Chemistry

The operational behavior of an electrolytic dissolver is considerably dependent upon the reactions which occur in the dissolver. An analysis of these reactions and their mechanisms may be made by measurement of current density as a function of electrode potential plus identification of the products formed. From an understanding of the electrode reactions, it will be possible to select optimum operating conditions. Further, the effect of cell and electrode geometry upon current density distribution is important to both cell design and operation. Most practical cell configurations are sufficiently complex that they are not directly amenable to theoretical calculation. A means of simulating these geometries should prove extremely useful.

Work in this area during the current quarter has been concerned with the measurement of potential-current relationships as a function of acidity, an investigation of the nitrate reduction reaction, and a simulation of current path distribution for various dissolver geometries.

Because of the interest in niobium for possible use as a cathode, and the knowledge that it can undergo hydrogen embrittlement under certain circumstances, a study of the hydrogen absorption by niobium when used as the cathode in an electrolytic dissolver was undertaken. Corrosion evaluation of other materials for general use in construction of an electrolytic dissolution system is also reported.

Electrolytic treatment of zirconium in nitric acid results in a disintegration (oxidation) of the metallic structure, rather than dissolution, but offers a method of freeing and recovering uranium from such a structure. Experimental work has resulted in recommended conditions for carrying out this oxidation in nitric acid, but favorable results and theoretical advantages from carrying out the reaction in neutral nitrate solution provide incentive to continue study of this system. In connection with this study, cathode potential measurements have given promise of furnishing a method for immediate detection of cathode corrosion during electrolytic dissolution.

A. Electrolytic Dissolution of Stainless Steel in Nitric Acid

1. Potential-Current Density Relationships in the Stainless Steel-Nitric Acid System

J. R. Aylward, Problem Leader; E. M. Whitener

Preliminary potentiostatic studies of the dissolution of Type 304 stainless steel in HNO_3 have revealed some interesting and unexpected features in the transpassive region.

A limiting current density is observed in the concentrated nitric acid solutions (curve 3 of Figure 21) whose value increases with decreasing acid concentration and increasing stirring rate. This

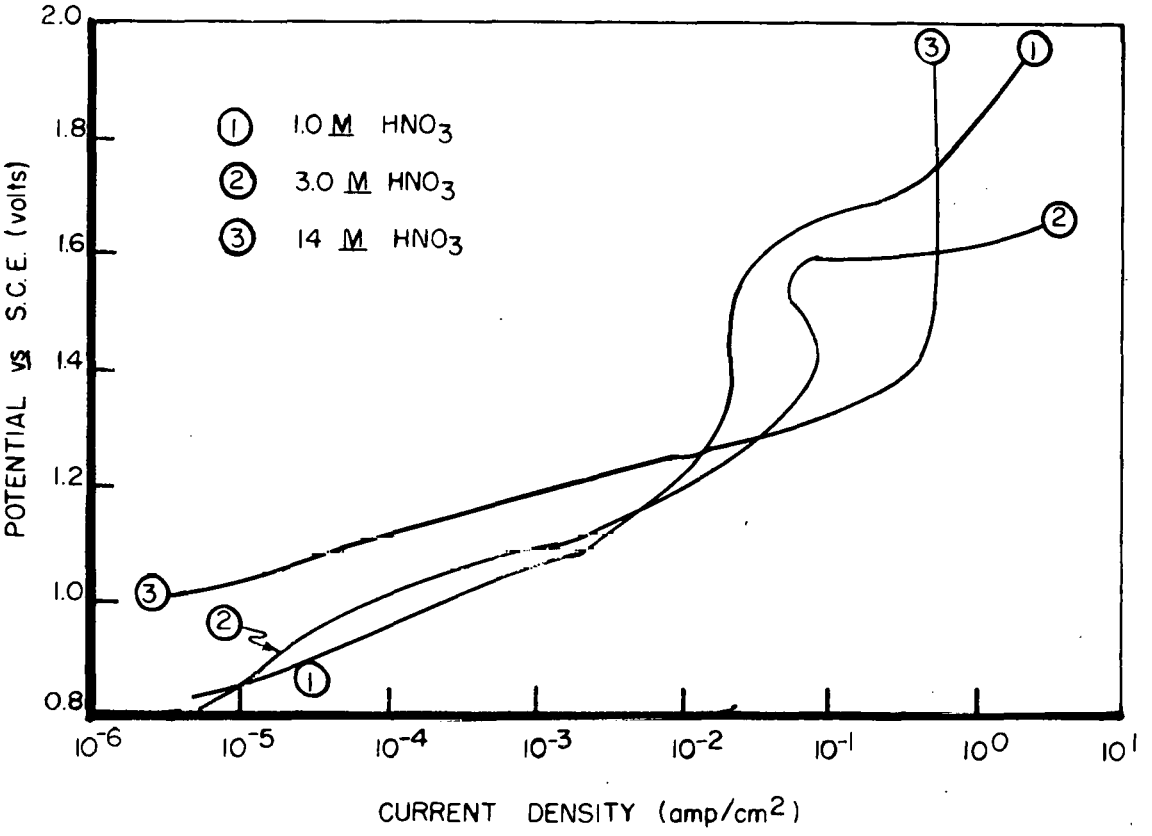

Fig. 21. Potential-Current Density Relationships at 25° C for Type 304 Stainless Steel in the Transpassive Region as a Function of Nitric Acid Concentration

limiting current density is due to concentration polarization or possibly to film formation such as occurs in electropolishing. True electropolishing is not observed, however, as the whole metal surface (although highly polished) contains many small craters.

At concentrations less than 6M HNO_3, different shapes are observed for the polarization curves. In 5M HNO_3, no limiting current density is observed up to 2 amp/cm^2. In 3M and 4M acid, the curves contained an "s" shape in the 1.2-1.6 volts region (curve 2 of Figure 21). This was more pronounced in the 3M, less so in the 4M, and not evident at all in 5M HNO_3. In 1M acid (curve 1 of Figure 21), this "s" region reverted to a limiting current density type curve which, it is felt, is the result of a secondary passivation phenomenon.

In all concentrations, the color of the solution at the liquid-metal interface became yellow at approximately 5 x 10^{-2} amp/cm^2. As the current density increased, the color changed to orange and finally to a reddish-brown at about 2 amp/cm^2, or at the limiting current density in the more concentrated solutions. Gas evolution was observed only in 1M nitric acid at potentials above +1.6 volts.

An extensive study of the transpassive region is being undertaken.

2. Electrolytic Reduction of Nitric Acid, J. R. Aylward

A literature search on the reduction of nitric acid was completed. Very little prior work of significance has been done on this system, mainly because of the complexity of the reaction and the experimental difficulties involved. The first stage in the reduction of nitric acid has been established with some certainty and is shown by the following reaction sequence:

$$HNO_3 + HNO_2 \longrightarrow N_2O_4 + H_2O \qquad (1a)$$

$$N_2O_4 \rightleftharpoons 2\ NO_2 \qquad (1b)$$

$$2(NO_2 + e \longrightarrow NO_2^-) \qquad (1c)$$

$$2(NO_2^- + H^+ \longrightarrow HNO_2) \qquad (1d)$$

with the overall reaction being

$$HNO_3 + 2H^+ + 2e \longrightarrow HNO_2 + H_2O \qquad (1)$$

Both step (1a) and (1c) have been claimed[10] to be slow, and the one actually controlling the overall reaction rate depends on the conditions of temperature, concentration of each species, and potential. It can be seen that the reduction of nitric acid to nitrous acid is also autocatalyzed, in that part of the nitrous acid formed in step (1d) is used up in step (1a). Because of this, the concentrations of the species taking part in the overall reaction (1) are continuously changing during the course of an experiment, so that reproducible results are impossible to obtain under ordinary circumstances. Further, no satisfactory analytical methods are available to determine the concentrations of the various species in solution.

Preliminary experiments are in progress to determine the rate of reaction (1c) at a gold cathode. Results to date indicate that this reaction is rapidly reversible (high exchange current), and attempts to measure the exchange current density will be made in the near future. The biggest problem in elucidating the reaction mechanism for the reduction of nitric acid is in devising experiments which allow the study of only one reaction without interference from others. Various experimental procedures are being developed and will be tried in an attempt to isolate the individual reactions.

3. Effect of Cell and Electrode Geometry on Current Density Distribution-Analog Simulation of Current Paths
J. R. Aylward, Problem Leader; R. E. Ohlin

The analog simulation of current paths in an electrolytic dissolver of the type being developed at the Idaho Chemical Processing Plant was undertaken to augment a concurrent mathematical study.

The current distribution at the cathode and anode of the dissolver may be calculated for cells having simple symmetrical geometries, i.e., a circular anode concentric with a larger, circular cathode. However, for cell geometries which are irregular with respect to the anode, calculation of current distribution becomes an extremely difficult task, and the geometries of interest are legion. These calculations were circumvented through the use of an analog simulation technique.

Conductive rubber sheeting of the type used in operating rooms to ground static electricity sufficed for the analog. Electrodes of the desired shape were applied to the rubber sheet by painting with conductive silver paint. All traces of solvent were removed by a 30-minute treatment in the vacuum oven at 85° C. The anode basket was simulated by cutting rubber sheeting from the analog along a circular arc. This procedure is allowed by the fact that the basket does not conduct current through the solution; its sole purpose is to provide electrical contact with the dissolving fuel element it contains. Holes in the anode basket are simulated by leaving the rubber sheeting intact, thus providing a conducting path for the current passing from the dissolving anode to the cathode. The dimensions of the analog were chosen to conform with those specified in early designs of the dissolver, i.e., a cathode diameter of 6 in. and an anode basket diameter of 5 in.

Initial experiments were designed to establish the applicability and performance of the rubber conductive sheeting as an electric analog. The sheeting proved to be satisfactory, and further studies were conducted to determine the changes in cathode current density resulting from the variation of the anode basket hole size and hole spacing when a central, circular electrode was used for the anode. Finally, the experimental setup was standardized and the geometry which was used for the remainder of the experiments was adopted (as shown in Figure 23). The anode basket consisted of equal areas of basket and holes, with a basket thickness of 1/8 inch.

The electrical lead to the anode was clipped to a copper wire soldered to a flat copper disk which in turn was compressed on to the silver conductive paint electrode. The cathode lead was fastened to the silver cathode by means of alligator clips. The analog was obtained by plotting equipotential lines in the following manner.

Experimental Method

The desired increment of the total voltage between the electrodes was measured with a Hewlett-Packard DC microvolt-ammeter, and the point of contact of the probe marked. The microvolt-ammeter was then used as a null indicator, and points of zero potential with respect to the reference point were plotted. In this way, lines of equipotential at definite fractions of the cell voltage were established.

These isopotential lines (hereafter denoted as isopots) serve to define the path of the current moving from one electrode to the other. The map of the isopots may be compared to a contour map in which the amount and direction of flow is determined by the gradient of the slope. The current path itself is perpendicular to the slope of the isopot at

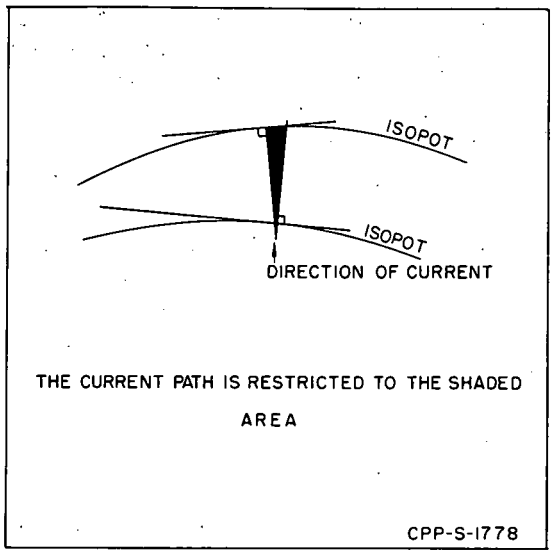

Fig. 22. Current Limitation Between Isopots

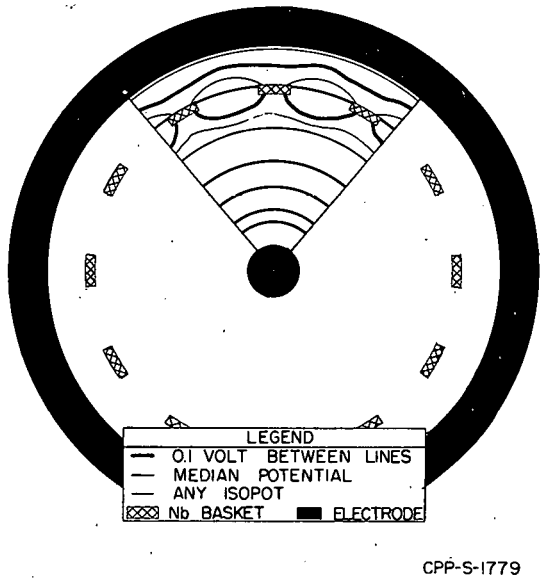

Fig. 23. Isopotential Lines in Sector of Uniform Geometry

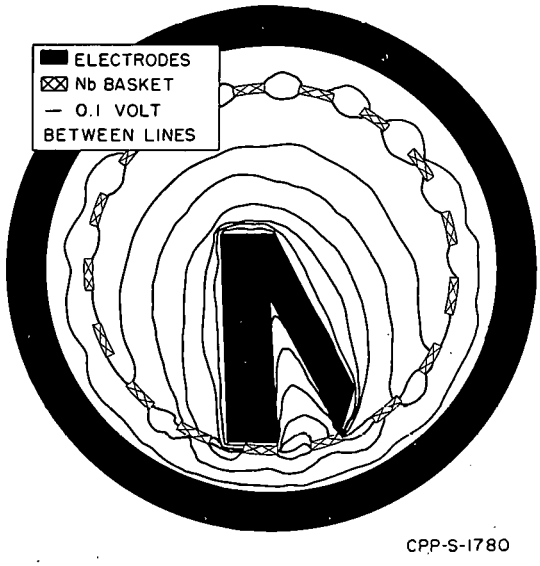

Fig. 24. Isopotential Lines in Non-Uniform Geometry

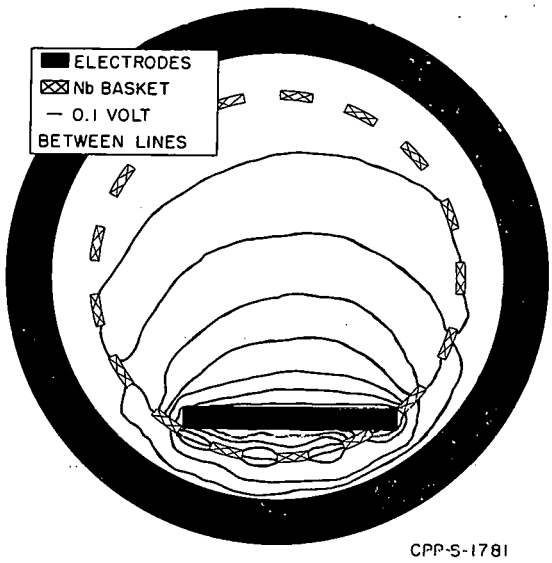

Fig. 25. Isopotential Lines in Non-Uniform Geometry

the point of intersection. The boundaries which limit the path that the current follows from one isopot to another are best understood by referring to the diagram shown in Figure 22. The current paths can be easily drawn visually within these limits, provided the isopots are reasonably close to one another.

The current distribution at the cathode is quite uniform for a cell having symmetrical electrode geometry (Figure 23) considering the conducting area available on the basket. A more interesting geometry is exhibited by the anode configuration shown in Figure 24. Several possible geometries are demonstrated: a basket hole partially blocked by the anode, a basket hole masked by the anode, and a surface receding from the basket hole. The concentration of isopots at the extremities of the anode suggests a much higher current density at these points, and one would expect the rate of dissolution at these points to be greatest. The current density at the cathode is also greatest along the circumference at the bottom of the figure, where the distance to the dissolving anode is shortest.

The anode in Figure 25 spans several holes and projects into a basket hole at one end. The current density at the anode is greatest at the ends and the surface closest to the cathode, whereas the current density at the cathode is greatest on the area in proximity to the entire dissolving anode. The overall current distribution of the cathode is concentrated at the bottom of the illustration with proportionately little current reaching the top.

A given analog holds for all geometries in which the relative sizes of the electrodes and basket are constant, i.e., for any magnification or condensation. An increase in basket porosity with no change in anode size would serve to smooth out local irregularities in the anode current density.

The analog simulation technique graphically provided additional information as to:

(a) Current distribution on the dissolver cathode
(b) Current distribution through the dissolver basket
(c) Current distribution on non-symmetrical anodes
(d) The actual path followed by the current in the dissolver

4. Embrittlement of Niobium Used as a Cathode
N. D. Stolica, Problem Leader; M. R. Bomar

Considerable attention has been given to the use of niobium as a cathodic construction material in an electrolytic dissolver. A literature search has revealed that niobium suffers hydrogen embrittlement under certain circumstances[11], and other metals including titanium[12], zirconium[13], nickel[14], and AISI 4340 steel[15] have been reported to absorb hydrogen when cathodically charged in various solutions. Of particular interest was the case in which tantalum suffered embrittlement when treated cathodically in a solution of 5M HNO_3 - 2M HCl[16].

Accordingly, a test was run to ascertain whether niobium would absorb hydrogen when charged cathodically in a nitric acid-stainless steel nitrate system. A coupon of niobium was used as the cathode in a batch dissolver for electrolytically dissolving stainless steel in 8M nitric acid. The solution was held at the boiling temperature; each day, 50 per cent by volume of the dissolver product solution was removed and replaced with 8M nitric acid. The cell current was 1 amp/cm^2 on the basis of the

cathode surface facing the dissolving anode. The back of the cathode was not masked, however, and the true current density was therefore somewhere in the range of 0.5 to 1.0 amp/cm^2. After an exposure of 1000 hours, the exposed niobium coupon (the cathode) and an unexposed coupon of the same material were submitted for hydrogen analysis to Metal Control Laboratories, Huntington Park, California.

Both specimens were reported to contain 29 PPM hydrogen. It has thus been shown that niobium does not absorb gross quantities of hydrogen when used as a cathode in electrolytic systems of the kind envisioned for stainless steel dissolution.

5. Corrosion Behavior of Electrolytic Dissolver Product Solution
N. D. Stolica, Problem Leader; C. E. May

In the evaluation of materials of construction for the electrolytic dissolution process, several stainless steels and other metals were tested in boiling dissolver product solution. The solution was prepared by the electrolysis of Type 304 stainless steel in 8M HNO_3. The analysis showed 1M HNO_3 and 75 g/l of dissolved stainless steel. The corrosion tests (which are continuing) had been underway for 59 days, with weekly observation periods, at the time of this writing. Whenever the corrosion rate for a metal was excessively large or became stabilized, the tests were discontinued.

TABLE 16

CORROSION IN ELECTROLYTIC DISSOLVER PRODUCT SOLUTION

Temperature: Boiling

Metal	Length of Test Days	Corrosion Rate mils/month
Type 347 Stainless Steel	59	3.5
Carpenter-20	59	3.55
Type 316 Stainless Steel	59	4.0
Type 304L Stainless Steel	59	5.0
Inconel	8	61.0
Titanium	52	0.002

It is seen that titanium shows excellent corrosion resistance, indicating that it may be useful for heat exchange surfaces in process evaporators. The stainless steels have tolerable corrosion rates, with Type 304L showing the highest rate; some pitting was found on the edge of the Type 304L coupons. Inconel is obviously undesirable for this use.

The corrosion rates for all stainless steels have been increasing slightly, so the tests are being continued.

B. Electrolytic Disintegration of Zirconium-Base Alloys

J. W. Codding, Problem Leader; M. R. Bomar

A series of tests has been run to define optimum conditions for the electrolytic treatment of zirconium-base alloys in nitric acid systems.

Nitric Acid Systems

Experiments in 4M and 8M nitric acid at 25° C, with and without the addition of 0.05M HCl, indicated no reaction up to 25 volts. Varying induction periods were noted at higher temperatures. In 8M nitric acid at 60° C, for example, a potential of 13 volts was sufficient to initiate a smooth reaction after some initial erratic current surges. It was noted that material appeared to form and slough off symetrically from the Zircaloy coupon at a uniform rate. The side facing away from the cathode was attacked at approximately the same rate as the side facing the cathode. This might indicate that the rate of attack is controlled by the rate at which the "scale" will slough off; the abnormal current surges sometimes observed when the reaction is initiated might also indicate this.

At 60° C and a potential of 13 volts in 8M nitric acid, the current density at a Carpenter-20 cathode with a Zircaloy-2 anode 1/4 inch away was approximately 0.45 amp/cm^2. The black material formed (scale) was submitted for X-ray analysis; the only crystalline phase detected was ZrO_2. This oxide accounted for approximately 73 per cent of the Zircaloy-2 which was removed from the anode. The solution contained 0.82 g/l of Zr, accounting for another 15 per cent. The current efficiency was not quantitatively determined, but from the time of the reaction and the ammeter reading, it was estimated to be 83 per cent.

When the temperature of dissolution was controlled at various levels, it was found, for the 8M nitric acid system, that Zircaloy-2 oxidized more rapidly in the temperature range of 55 to 75° C than at temperatures from 75 to 100° C or at temperatures less than 55° C. The temperature is difficult to control at less than 55° C because the reaction, once initiated, is very exothermic. Table 17 shows the results of these experiments. The optimum conditions for zirconium disintegration in a nitric acid system are: dissolvent, 8M nitric acid; temperature, 60° C; cell potential, about 13 volts. These conditions produce an average rate of penetration of about 0.6 mm/hr at essentially 100 per cent current efficiency.

Neutral Systems

The disintegration of Zircaloy-2 in neutral nitrate solutions is currently being studied. Solutions used have been 8M sodium nitrate, 8M ammonium nitrate, and 2.3M aluminum nitrate. These neutral solutions are of interest for several reasons: 1) the low solubility of zirconium species in these systems should allow for complete precipitation of the disintegrated Zircaloy, thus effecting a uranium-zirconium separation; 2) cathodic corrosion should be materially reduced by operating in a non-acidic system; and 3) the hazard of a nitric acid explosion due to

TABLE 17

EFFECT OF TEMPERATURE ON RATE OF ELECTROLYTIC DISINTEGRATION OF ZIRCALOY-2

Approximate Temperature	Average Rate of Disintegration	Average Current Efficiency	Cell Voltage
45° C	0.44 mm/hr	98 per cent	13
55	0.64	99	13
65	0.60	99	13
75	0.60	98	13
85	0.57	99	13
95	0.41	98	13
100	0.35	95	13

the presence of the Zr-U epsilon phase should be eliminated. Preliminary work has shown that in such systems Zircaloy-2 can be disintegrated and precipitated nearly quantitatively as ZrO_2. Periodic addition of nitric acid is required to replenish the nitrate lost during the reaction. The sodium nitrate system will be studied further.

C. Single Electrode Potential Measurements as an Indication of Cathode Corrosion, J. W. Codding, Problem Leader; M. R. Bomar

Cathodic potential measurements were made with a Luggin probe during the nitric acid experiments described in Part B. These tests to date have employed Carpenter-20 cathodes. Single electrode potentials have been measured during dissolution, and cathodic corrosion rates determined. Table 18 shows the results of this preliminary study. The Carpenter-20 cathode shows a potential of 0.95 volt when immersed in nitric acid, with no current passing. The current density for the work shown in Table 18 was about 1 amp/cm^2. In one additional experiment at 7M sodium nitrate and 1.0M nitric acid, cathode corrosion was over 200 mils per month with a single electrode potential of -0.45 volt.

TABLE 18

CORRELATION OF SINGLE ELECTRODE POTENTIAL AND CATHODIC CORROSION DURING ELECTROLYTIC DISINTEGRATION OF ZIRCALOY
(Dissolvent, 8M HNO_3; Carpenter-20 Cathode)

Temperature (°C)	Corrosion Rate (mils/month)	Cathodic Potential with Respect to Hydrogen Electrode (volts)
100	12.9	0.07
95	11.4	0.10
95	10.0	0.14
85	10.0	0.11
75	7.7	0.17
65	7.0	0.17

A correlation of cathode potential and cathode corrosion in an operating dissolver could be of considerable process significance in indicating, instantaneously, when corrosive operating conditions exist in the dissolver. These experiments are preliminary in nature and will be expanded in the next quarter.

VII. THE ARCO PROCESS - DISSOLUTION OF FUEL ALLOYS IN MOLTEN CHLORIDES

Section Chief: H. T. Hahn, Chemical Research

The ARCO Process employs molten lead chloride as a solvent for reactor fuel alloys. The product salt contains uranium chloride together with excess lead chloride and the alkali, alkaline earth, and rare earth fission products. Satisfactory uranium recovery from the salt matrix has been achieved with HNO_3 leaching.

Efforts were directed this past quarter toward modification of the original ARCO Process so as to permit dissolution of UO_2 reactor fuel at relatively low temperatures (500-550° C). Since zirconium and Zircaloy cladding can be readily dissolved by the original ARCO Process[17], and stainless steel cladding can be dissolved by passing chlorine through the melt at 520° C[18], successful dissolution of UO_2 in $PbCl_2$ would provide a means for integral dissolution of this type fuel. A program has also been initiated to study the behavior of niobium and ruthenium in fused chloride melts of interest.

Investigation of the $PbCl_2$-Cl_2 system as a possible medium for dissolution of UO_2 revealed that only a very low dissolution rate was attainable in this system, even at 800° C. However, by addition of copper to the system as either CuCl or copper metal, more than adequate dissolution rates were achieved at 550° C. The dissolution can also be performed adequately at 430° C in a $PbCl_2$-$CdCl_2$-CuCl-Cl_2 system.

The dissolution rate of niobium in lead chloride has been measured in the 600-700° C range.

A. Dissolution of UO_2 in the $PbCl_2$-Cl_2 System

E. M. Vander Wall, Problem Leader; D. L. Bauer

The rate of dissolution of UO_2 in molten $PbCl_2$ is negligible; the dissolution rate at 800° C was found to be only 0.3 $\mu g\ cm^{-2}\ min^{-1}$ [1]. In anticipation of a greater dissolution rate, the $PbCl_2$-Cl_2 system was investigated as a possible dissolution medium for UO_2. The apparatus used in these experiments was similar to one previously described[18]. The molten $PbCl_2$ (20 g) was contained in a Pyrex glass tube and supported by a 20 mm-diameter medium-porosity glass frit through which chlorine was introduced into the melt. The UO_2 used was in the form of cylindrical pellets (0.9 cm diameter, 0.9 cm high, density = 10.28, calculated surface area = 3.35 cm^2). As an indication of the chlorine flow rate, a glass capillary flowmeter was used. The chlorine which passed through the melt was collected in a KI solution, which was then titrated with $Na_2S_2O_3$ to determine the amount of Cl_2 not used. The amount used is determined by the stoichiometry of the respective experiment.

The experiments were conducted at 550° C for periods from 30 to 60 minutes. The Cl_2 flow rates varied from 19 to 79 mg/min, and the resultant dissolution rates varied from 0.062 to 0.242 $mg(UO_2)cm^{-2}min^{-1}$. In order to compensate for the variation in chlorine flow rates for the several experiments, the dissolution rate was divided by the flow rate.

This yielded an average rate constant, $k = 0.0028 \pm 0.0004$ $mg(UO_2)$ $cm^{-2}min^{-1}/mg(Cl_2)min^{-1}$, for the expression

$$-\frac{d(UO_2)}{dt} = k\,(Cl_2)(UO_2 \text{ apparent area}).$$

The dissolution rates obtained in the $PbCl_2$-Cl_2 system were 100 to 1000 times greater than those observed in $PbCl_2$ alone. However, these rates are still too low to be practical in a dissolution process.

B. Dissolution of UO_2 in the $PbCl_2$-Cl_2 System Catalyzed by Copper

E. M. Vander Wall, Problem Leader; D. L. Bauer

In order to effect a suitable dissolution rate of UO_2 in a modification of the original ARCO Process, it was felt that a catalyst might be employed to serve as a carrier for chlorine in the $PbCl_2$-Cl_2 system. A polyvalent cation was sought, and, since at these temperatures CuCl is the stable form of the copper chlorides, it was a likely candidate for a catalyst. Small amounts of copper were added to 20 g of molten $PbCl_2$, then Cl_2 was passed through the melt until the copper metal dissolved. The UO_2 pellet was then introduced into the apparatus, which was the same as used in the $PbCl_2$-Cl_2 system, and the Cl_2 flow through the melt was continued for periods from 10 to 30 minutes. The presence of copper in the system enhanced the dissolution rates of UO_2 greater than 100 fold. Using pellets similar to those used in the $PbCl_2$-Cl_2 system, it was possible to achieve average dissolution rates over a 30-minute period of up to 69 $mg(UO_2)cm^{-2}min^{-1}$ with a chlorine flow rate of 64 mg/min and an initial 10 mole per cent copper concentration.

A dissolution was attempted in a mixture of molten $PbCl_2$ and CuCl at 550° C; no appreciable dissolution was observed which established the fact that chlorine was necessary for the reaction.

Chloride analyses of entire reaction mixtures, combined with the analyses of the uranium present, indicated that one mole of chlorine combined with one mole of UO_2 during dissolution, and that the most probable reaction product was UO_2Cl_2.

Since it was apparent that the dissolution rate was a function of the chlorine flow rate, a series of experiments was performed in which the copper concentration was maintained relatively constant and UO_2 pellets of the same initial calculated area were used. The results are presented in Figure 26 and indicate that the dissolution rate has a first order dependency on the chlorine flow rate. The slight concavity of the curve will be checked at higher chlorine flow rates.

During the dissolution process, the UO_2 pellets not only decreased appreciably in size but also often shattered into several pieces. This made the determination of the surface area during dissolution practically impossible. In order to achieve a more nearly reproducible surface area, finely divided UO_2 was substituted for the pellets. The material used was between 30-35 mesh (average diameter 0.55 mm) and had a density of 10.18 g/cc. The true surface area of this material has not been determined, but the same quantity of material was used in each experiment to

give approximately the same initial surface area.

The effect of the copper concentration on the dissolution rate of UO_2 was determined by use of this 30-35 mesh material. The area during dissolution was obtained by averaging the initial and final areas which were calculated on the assumption that all the particles were spheres and had the same diameter, and that during dissolution the diameters all decreased uniformly.

The data from these experiments are presented in Figure 27, where the dissolution rate is plotted versus the molality of the copper. Molality was used because it can be defined in terms of the solvent, $PbCl_2$, and therefore remains constant during dissolution even though other solutes are introduced.

The results indicate that during a 10-fold change in the copper concentration, the dissolution rate is dependent on approximately the 1/2 power of the copper concentration. The equation which expresses the dissolution rate is

$$-\frac{d(UO_2)}{dt} = k\,(Cl_2)(Cu)^{1/2},$$

where k is expressed in $mg(UO_2)min^{-1}/(mg(Cl_2)min^{-1})(Cu\ molality)^{1/2}$.

The average value for k with its standard deviation is 4.83 ± 1.07 $mg(UO_2)min^{-1}/(mg(Cl_2)min^{-1})(Cu\ molality)^{1/2}$ if one considers all the experiments (21) in which both pellets and finely divided UO_2 were used. The average value for k in experiments where only UO_2 pellets were used is 4.37 ± 0.74. The area of the UO_2 surface is included in the k.

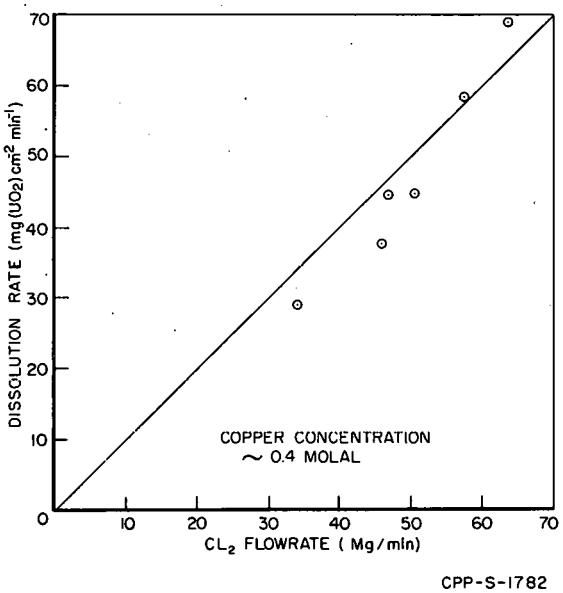

Fig. 26. Dissolution Rate of UO_2 in Molten Lead Chloride at 550° C as a Function of Cl_2 Flow Rate

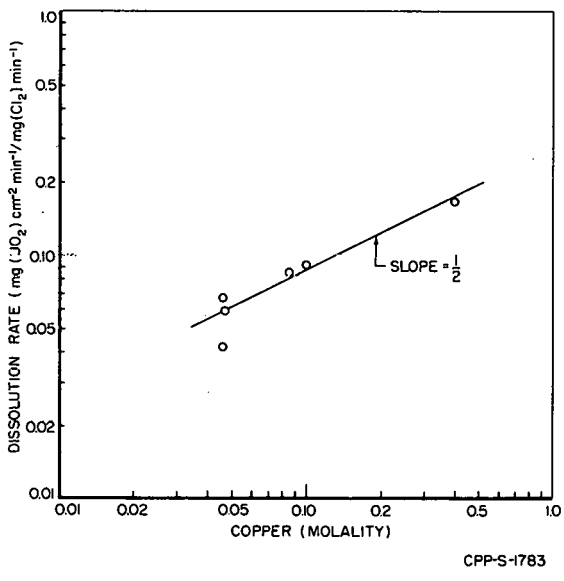

Fig. 27. Dissolution Rate of UO_2 in Molten Lead Chloride at 550° C as a Function of Copper Concentration

In the experiments conducted so far, it has been found that the dissolution rate is almost independent of the surface area used. This may be due either to the inability to determine areas accurately, or to some rate controlling step in the dissolution mechanism. Additional experiments are being conducted to clarify this situation.

In an attempt to perform these dissolutions at lower temperatures, a molten mixture of 60.2 m/o $PbCl_2$-25.8 m/o $CdCl_2$-14.0 m/o CuCl was used at 430° C. The Cl_2 flow rate during the 30-minute dissolution period was 34 mg/min, and 2.10 g of the original 5.83 of UO_2 pellet dissolved. The pellet remained intact during the dissolution, and the average dissolution rate based on the initial calculated area of the pellet was 21 $mg(UO_2)cm^{-2}min^{-1}$.

C. Dissolution of Niobium in Molten Lead Chloride
E. M. Vander Wall, Problem Leader; J. L. Teague

An investigation of niobium behavior in the molten lead chloride system has been initiated. The apparatus consisted of a 3-inch crucible furnace with thermostatic temperature control. Experiments at 600° C were controlled to ± 5° C, and experiments at 625-700° C were controlled to ± 2° C. Dissolutions were carried out in 4-inch Pyrex test tubes (or 6-inch Vycor tubes for 700° C runs) containing approximately 7-1/2 g lead chloride. All 700° C, 650° C, and 625° C experiments and about one-half the 600° C experiments were carried out under a static blanket of argon. The presence of the argon blanket had no appreciable effect on the dissolution rate.

A plot of weight loss versus temperature (Figure 28) shows an increase of the rate with increasing temperature, and a decrease of overall rate with increasing contact time. The ranges indicated include all experimental results for a given indicated time. Experiments with a contact time of 30 min. show an average rate of 0.122 mg/(min)(cm^2) at 600° C, 0.239 mg/(min)(cm^2) at 625° C, 0.223 mg/(min)(cm^2) at 650° C, and 0.556 mg/(min)(cm^2) at 700° C. For contact times of 3 hours, the corresponding average rates are 0.048 mg/(min)(cm^2) at 600° C, 0.094 mg/(min)(cm^2) at 625° C, 0.16 mg/(min)(cm^2) at 650° C, and 0.24 mg/(min)(cm^2) at 700° C.

Based upon the 3-hour data, the reaction thus appears to have an activation energy of 28.8 Kcal/mole over the temperature range 600-700° C.

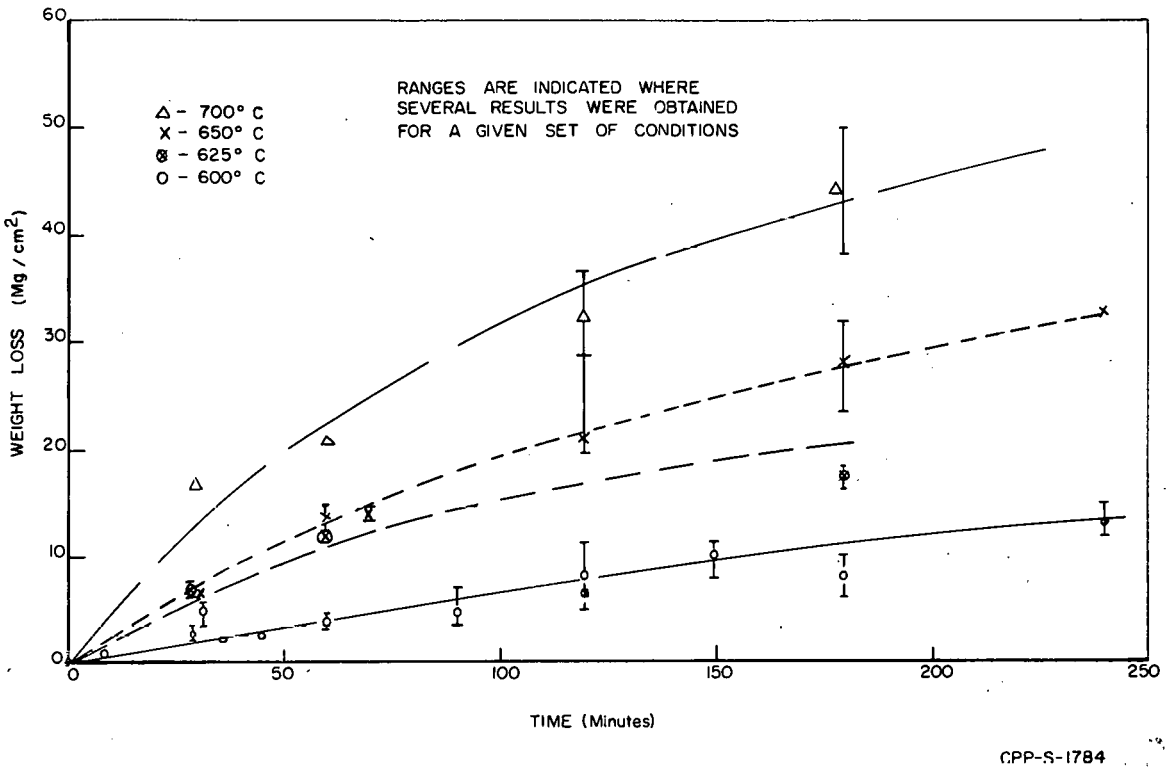

Fig. 28. Weight Loss of Niobium in Lead Chloridc as a Function of Temperature

VIII. EQUIPMENT DEVELOPMENT

Section Chief: M. E. Weech
Process Engineering

Two equipment development projects currently in progress are aimed at simplifying ICPP operations, reducing maintenance and operating expense, and increasing the safety of the processing operation. Success in preliminary operation of a pilot model led to installation of a direct air pulsing system on the first cycle extraction column to replace the remote head pulser system.

Existence of nuclear safety hazards associated with equipment incorporating non-geometrically safe components has led to design of a boron stainless steel (neutron poisoning) cartridge for insertion in a large-diameter vessel. Neutron multiplication tests will provide additional data for refinement of design and adaptation to several locations in the processing equipment

A. Direct Air Pulsing of Extraction Columns

D. K. MacQueen, Problem Leader; R. S. P'Pool

The mechanical-hydraulic pulsers currently used at the ICPP have been a major source of plant operating problems. A system using direct air pulsing is under development to provide a more reliable method of pulsing extraction columns. The elimination of in-cell maintenance requirements is the major advantage of the air pulser system. Simplicity of operation, elimination of nearly all moving parts, low cost, and the ease of pulse frequency and amplitude adjustment are the remaining primary reasons for the present development effort.

Description of Operation

Figure 29 shows the basic components of an experimental air pulser system which has been built and tested. By alternately operating valves V_1 and V_2, air pressure is applied and relieved, cyclically, to the top of the pulse leg. Air pressure forces the fluid in the pulse leg down, raising the fluid in the column. When the air pressure on the pulse leg is released, the unbalanced hydrostatic forces raise the pulse leg liquid level, lowering the fluid in the column. The distances X and ΔX shown in Figure 29 represent the average height of liquid in the pulse leg and the amplitude of the pulse in the leg. The column pulse amplitude is, of course, less than the leg pulse amplitude by the ratio of leg to column cross sections. By adjustment of the valve operating cycle time and the magnitude of the applied air pressure, the frequency and amplitude of the column pulse can be regulated. The only moving parts are the operating valves, V_1 and V_2, and all parts subject to failure can be located in accessible areas.

Experimental Air Pulser System

Although the air pulser system is basically quite simple, the design of any given installation is complex. The system is always in a transient condition, and the governing differential equations cannot be solved by

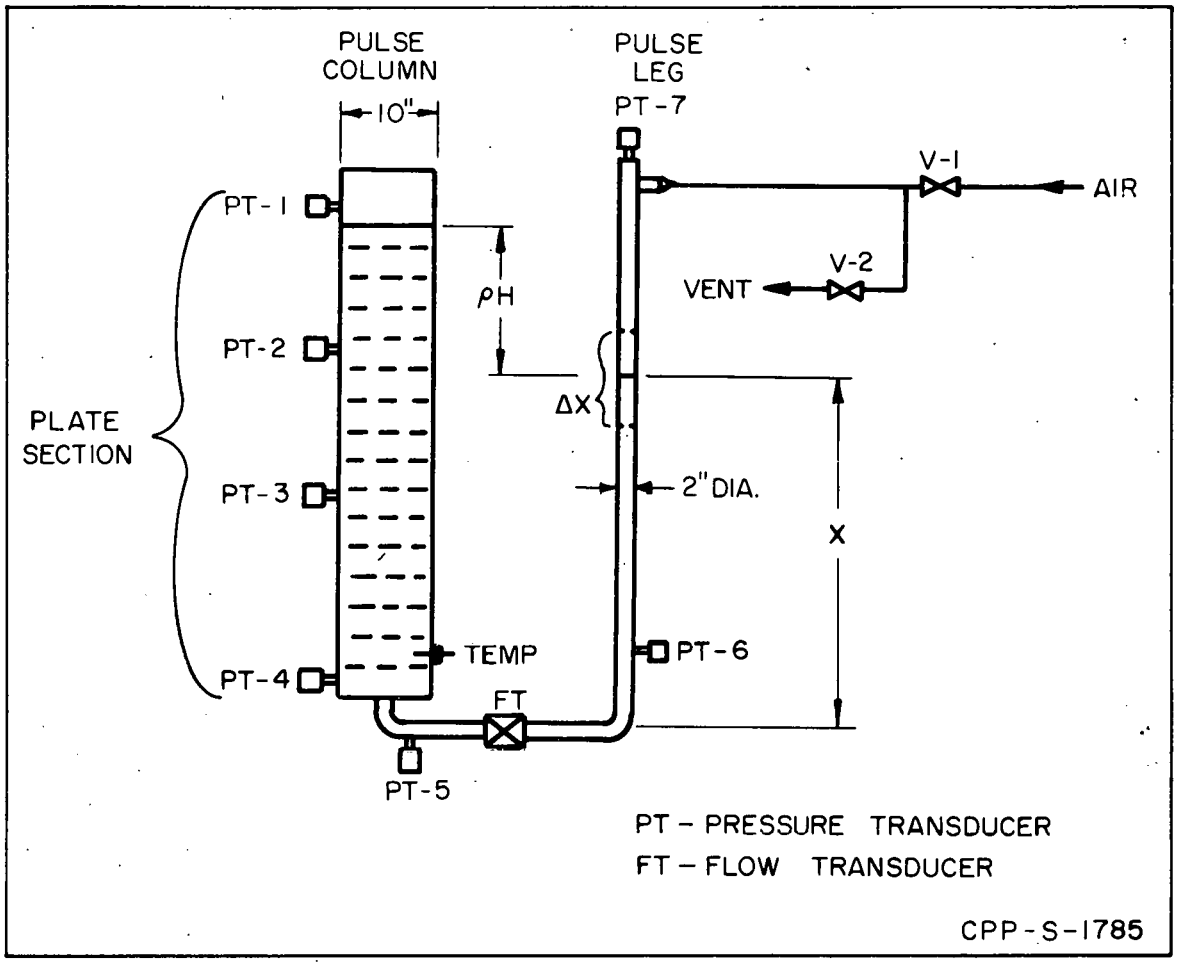

Fig. 29. Schematic of Air Pulser Test System

classical means. A program for an analog computer was developed by incorporating certain simplifying assumptions, but experimental data will be required to verify or modify the assumptions made. The experimental pulser, shown in Figure 29, was built to provide the required data.

The experimental system is based on a 10-inch i.d. perforated plate column with a 20-foot cartridge length. The pulse leg is fabricated from 2-inch Pyrex glass to permit visual observation of the liquid height in the leg. Seven pressure transducers are provided to permit following the pressure cycles at various points in the system. An electromagnetic flowmeter is installed between the pulse leg and the column to provide instantaneous flow rate data. Demodulating and differentiating circuits were designed and installed to remove the 60-cycle component of the flowmeter signal and to provide both velocity and acceleration outputs directly. Both the pressure transducer signals and the demodulated flowmeter signals can be fed to either a Sanborn recording oscillograph or an oscilloscope.

The test unit air supply and operating valve system are shown in Figure 30. The pressure in the air reservoir is regulated by a

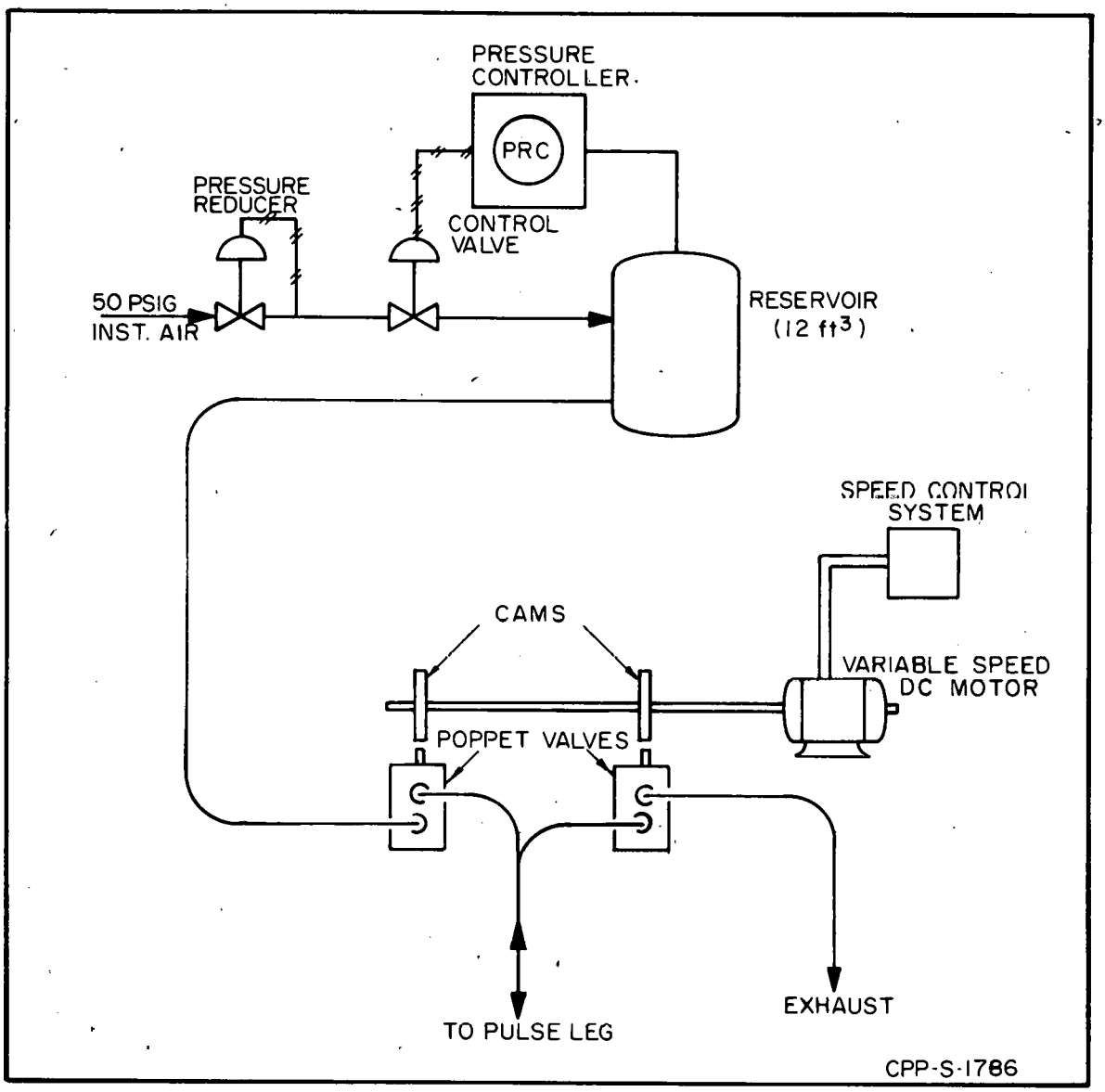

Fig. 30. Air Pulser Air Supply System

conventional pressure controller. The inlet and outlet valves are a specially designed type of poppet valve (Hydro-Aire Company, Part No. 35-595). The valves are operated by an adjustable tandem cam unit, driven by a variable speed motor. The pressure set on the air reservoir and the speed of the cam drive motor determine the column pulse amplitude and frequency.

The test unit has been installed and operated, but electronic measurement problems have so far prevented making a complete data run. Preliminary checkouts with water and an abbreviated 2-phase test have been very encouraging.

Plant Air Pulsers

The excellent results obtained during the preliminary testing of the experimental air pulser, and the poor operating history of the mechanical-hydraulic pulsers, made it very probable that air pulsers would replace the mechanical pulsers in the very near future. The need for an improved pulser was sufficiently urgent to proceed with a full-scale plant test before completion of the development program. Air pulsers are being installed on the A, B, and C columns of the high-capacity TBP extraction system. The A column installation is being completed, but only the in-cell portions of the B and C column units are being installed now. In each case, the air pulser is placed in parallel with the existing mechanical pulsers. Should the plant tests with the A column indicate that the air pulsers do not operate up to expectations, the mechanical pulsers can continue in use. If the A column tests are successful, the B and C column air pulser installations can be completed without re-entering the cells.

In the absence of experimental data to permit refinement of the design equations, the plant air pulsers were of necessity installed as almost identical copies of the test unit. The same valve, cam, and drive system was used for the air supply, and a 2-inch pipe was used for the pulse leg. The major differences are the inclusion in the plant units of devices such as seal loops and solenoid shutoff valves to prevent the backup and escape of radioactive plant column fluids, and the omission of the flow and pressure transducers used on the experimental column.

To provide a guide for operation, an analog computer run was made for the plant A column pulser, using the simplifying assumptions previously made for the experimental column. The results are shown in Figure 31. As a further check, 2-phase runs on the test unit were made. Since the electronic flowmeter circuits were not functioning properly, only frequency, air pressure, and pulse amplitude could be measured. The experimental points are also shown in Figure 31. The analog runs were made with column organic holdups of 20, 30, and 40 per cent to cover the anticipated plant operating range. The organic holdup of the experimental unit could not be determined accurately, but was probably between the 20 and 40 per cent limits. The excellent agreement between the calculated and observed values (the test unit simulates the A column fairly closely) was a major factor in the decision to proceed with the plant installation now.

B. Large Vessel Criticality Control

D. K. MacQueen, Group Leader; G. K. Cederberg

The safe containment of enriched uranium solutions in large-diameter vessels has been a continuous problem in uranium processing plants. Adherence to stringent procedures and the use of small-diameter, geometrically-safe vessels for the accumulation of concentrated uranium solutions have been necessary to maintain safe conditions during uranium processing at the ICPP.

The use of boron-containing Raschig ring packing has been

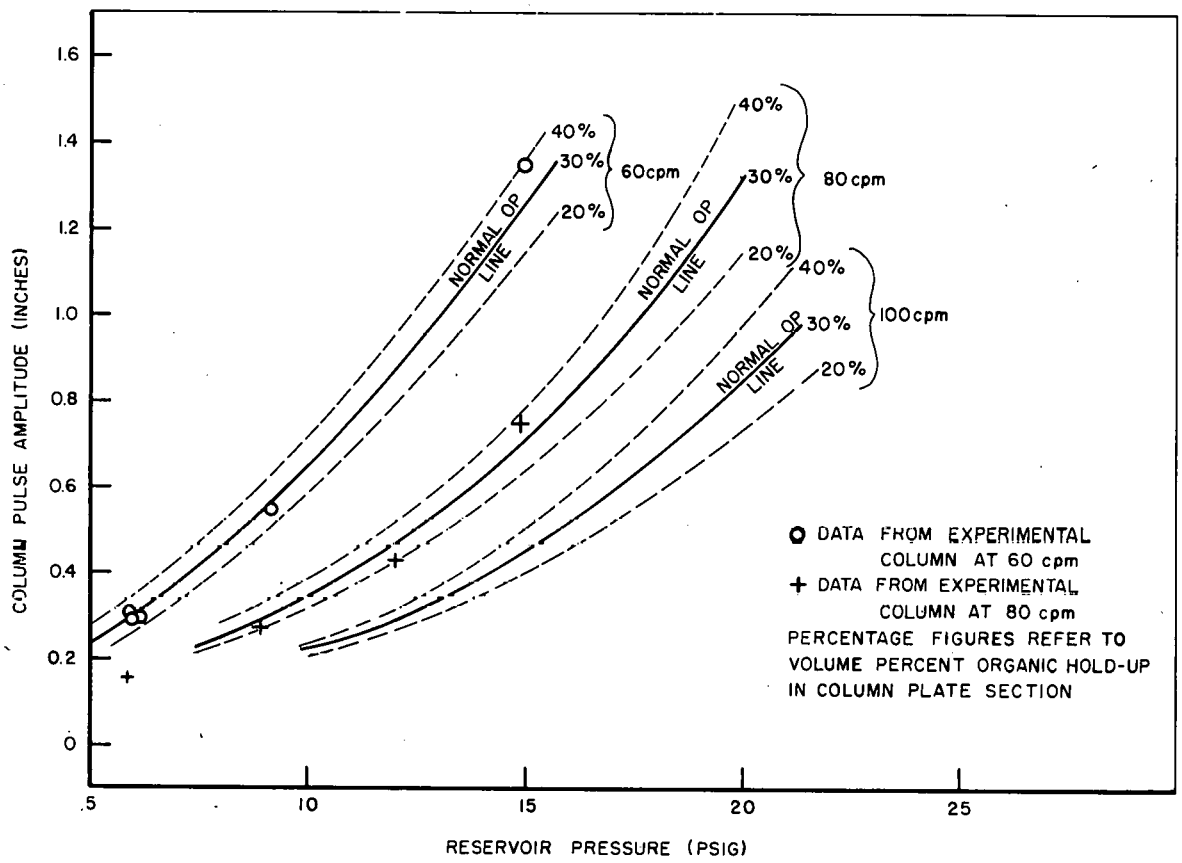

Fig. 31. Extraction Column Air Pulser Settings

investigated[1,6], and Pyrex glass rings have been found to be satisfactory for some applications[19] where large-diameter vessels must be poisoned to contain, safely, high concentrations of enriched uranium. Boron stainless steel rings appear more applicable for general use in ICPP vessels than do Pyrex rings, because of their greater mechanical strength and corrosion resistance, but any Raschig ring packing has the disadvantage of having a multitude of small interstices that could hold up radioactive solids.

In view of the inherent disadvantage of loose, randomly-oriented packing, study was initiated on the design of a prefabricated cartridge which would offer more efficient utilization of the neutron poisoning material and would minimize the holdup problem. Arrangements have been made to run neutron multiplication tests on a test vessel with such a cartridge at the Rocky Flats Plant of the Dow Chemical Company.

Of several possible cartridge designs, one with vertical flat plates appeared most desirable, because it would be easiest to fabricate, would offer minimum holdup, and should provide the most usable data from neutron multiplication tests. Boron stainless steel plates, containing about 1.1 per cent natural boron, are being fabricated into a cartridge about 48 inches high that will fit into a 36-inch diameter vessel. This cartridge was designed so that the spaces between the plates can be

varied between 1 inch and 2-1/2 inches. This range of plate spacing brackets the maximum safe plate spacing as determined by a modified two-group, single region calculation on an IBM 704 computer. The results of the proposed neutron multiplication tests should permit refinement of the parameters used in the computer program and increase the precision of similar calculations in the future.

IX. REPORTS AND PUBLICATIONS ISSUED DURING THE QUARTER

1. Vander Wall, E. M., H. T. Hahn, and D. L. Bauer
Salt-Phase Chlorination of Reactor Fuels: II. ARCO Process Definition and Scoping Studies, IDO-14525, October 28, 1960

2. McLain, M. E. and D. W. Rhodes
Stainless Steel Process Wastes: I. Removal of Alloy Metals from Waste Solutions by Mercury Cathode Electrolysis, IDO-14533, September 30, 1960

3. Paige, B. E.
Simplified Method for the Calculation of Fission-Product Activities and Concentration, IDO-14542, December 12, 1960

X. REFERENCES

1. Bower, J. R., Chemical Processing Technology Quarterly Progress Report, July-September 1960, IDO-14540

2. Paige, B. E., Barium Fluozirconate Precipitation from Hydrofluoric Acid-Zirconium Fuel Reprocessing Solutions, Part I. Process Chemistry, IDO-14511, September 20, 1960

3. Stevenson, C. E., Technical Progress Report for July through September, 1959, Idaho Chemical Processing Plant, IDO-14509

4. Blumenthal, Warren B., The Chemical Behavior of Zirconium, pp. 314-318, D. Van Nostrand Company, Inc., New York, 1958

5. Stevens, J. I., Idaho Chemical Processing Plant Technical Progress Report: Radioactive Waste Disposal Projects, January-March 1960, IDO-14530

6. Bower, J. R., Chemical Processing Technology Quarterly Progress Report, April-June 1960, IDO-14534

7. MacQueen, D. K. and J. I. Stevens, Design Bases for ICPP Waste Calcining Facility, IDO-14462, April 22, 1959

8. Bower, J. R., Idaho Chemical Processing Plant Technical Progress Report, January-March 1960, IDO-14520

9. Youngblood, E. L., Development of an Electrolytic Cell for Removal of Nickel from HRT Fuel Solutions, ORNL-2932 (1960)

10. Vetter, K. J., Z.Phys.Chem., 194, 199 (1950)

11. Miller, G. L., Metallurgy of the Rarer Metals, No. 6, Tantalum and Niobium

12. Hammond, J. P., CF-58-2-77

13. Shannon, D. W., HW-55460

14. Smialowski, M., The Effect of Cathodically Evolved Hydrogen on Iron and Nickel, Chem. and Ind., No. 35, 1078-1083 (1959)

15. Troiana, A. R., Corrosion Failure of High Strength Steels, Corrosion, 15, No. 4, 207T-212T (1959)

16. Peterson, C. L., P. D. Miller, and E. L. Whit, Materials of Construction for Headend Processes, Ind. Eng. Chem., 51:1, 32-37

17. Hahn, H. T. and E. M. Vander Wall, Salt Phase Chlorination of Reactor Fuels, I. Dissolution of Zirconium Alloys in Lead Chloride, IDO-14478 (1959)

18. Vander Wall, E. M., H. T. Hahn, and D. L. Bauer
Salt Phase Chlorination of Reactor Fuels, II. ARCO Process Definition and Scoping Studies, IDO-14525 (1960)

19. Bidinger, G. H., C. L. Schuske, and D. F. Smith, RFP-201

PHILLIPS
PETROLEUM
COMPANY

ATOMIC ENERGY DIVISION